A. AGHNAIYA

VARIATIONAL MODE DECOMPOSITION BASED RADIO FREQUENCY FINGERPRINTING OF BLUETOOTH DEVICES

THE GRADUATE SCHOOL OF NATURAL AND APPLIED SCIENCES
OF
ATILIM UNIVERSITY

ALGHANNAI AGHNAIYA

DOCTOR OF PHILOSOPHY THESIS
IN
MODELING AND DESIGN OF ENGINEERING SYSTEMS (MAIN FIELD OF STUDY: ELECTRICAL ELECTRONICS ENGINEERING)

DECEMBER 2019

ATILIM UNIVERSITY 2019

VARIATIONAL MODE DECOMPOSITION BASED RADIO FREQUENCY FINGERPRINTING OF BLUETOOTH DEVICES

A THESIS SUBMITTED TO
THE GRADUATE SCHOOL OF NATURAL AND APPLIED SCIENCES
OF
ATILIM UNIVERSITY

BY

ALGHANNAI AGHNAIYA

IN PARTIAL FULFILLMENT OF THE REQUIREMENTS
FOR
DOCTOR OF PHILOSOPHY
IN
MODELING AND DESIGN OF ENGINEERING SYSTEMS (MAIN FIELD OF STUDY: ELECTRICAL ELECTRONICS ENGINEERING)

DECEMBER 2019

Approval of the Graduate School of Natural and Applied Sciences, Atilim University.

_____

Prof. Dr. Ali Kara
Director

I certify that this thesis satisfies all the requirements as a thesis for the degree of **Doctor of Philosophy in Modeling and Design of Engineering Systems, Atilim University.**

_____

Prof. Dr. Ender Keskinkılıç
Head of Department

This is to certify that we have read the thesis VARIATIONAL MODE DECOMPOSITION BASED RADIO FREQUENCY FINGERPRINTING OF BLUETOOTH DEVICES submitted by ALGHANNAI AGHNAIYA and that in our opinion it is fully adequate, in scope and quality, as a thesis for the degree of Doctor of Philosophy.

_____

Prof. Dr. Ali Kara
Supervisor

Prof. Dr. Bülent Tavlı
Electric and Electronics Eng. Depart, TOBB Univ. _____

Prof. Dr. Ali Kara
Electric and Electronics Eng. Depart, Atilim Univ. _____

Assoc. Prof. Dr. Mehmet Ünlü
Electric and Electronics Eng. Depart, TOBB Univ. _____

Asst. Prof. Dr. M. Efe Özbek
Electric and Electronics Eng. Depart, Atilim Univ. _____

Asst. Prof. Dr. Özgür Ergül
Electric and Electronics Eng. Depart, Atilim Univ. _____

Date: *26 December 2019*

I hereby declare that all information in this document has been obtained and presented in accordance with academic rules and ethical conduct. I also declare that, as required by these rules and conduct, I have fully cited and referenced all material and results that are not original to this work.

ALGHANNAI, AGHNAIYA :

Signature:

ABSTRACT

VARIATIONAL MODE DECOMPOSITION BASED RADIO FREQUENCY FINGERPRINTING OF BLUETOOTH DEVICES

Aghnaiya, Alghannai

PhD., Modelling And Design Of Engineering Systems

Supervisor: Prof. Dr. Ali Kara

December 2019, 77 pages

In this thesis, we evaluated the performance of RF fingerprinting method based on variational mode decomposition (VMD). Radio frequency fingerprinting (RFF) is based on identification of unique features of RF transient signals emitted by radio devices. RF transient signals of radio devices are short in duration, non-stationary and nonlinear time series. For this purpose, VMD is used to decompose Bluetooth (BT) transient signals into a series of band-limited modes, and then, the transient signal is reconstructed from the modes. Higher order statistical (HOS) features are extracted from the complex form of VMD-reconstructed transients and VMD-modes. Then, Linear Support Vector Machine (LVM) classifier is used to identify BT devices. The method has been tested experimentally with BT devices of different brands, models and series. The classification performance shows that VMD-reconstructed transients method achieves better performance (at least 8% higher) than time-frequency-energy (TFED) distribution based methods such as Hilbert-Huang Transform. This is demonstrated with the same dataset but with smaller number of features (nine features) and slightly lowers (2-3 dB) SNR levels. For the same dataset the classification performance demonstrates that VMD-modes method achieves better performance (4% higher) than VMD-reconstructed transient method.

Keywords: Variational mode decomposition, Bluetooth signals, Specific emitter identification, Feature extraction, Classification.

ÖZ

VARYASYONEL KİP AYRIŞTIRICI KULLANARAK BLUETOOTH CİHAZLARIN RADYO FREKANS PARMAK İZİ ÇIKARIMI

Aghnaiya, Alghannai
Soyad, Ad
Doktora, Mühendislik Sistemlerinin Modellenmesi ve Tasarımı Bölümü
Tez Yöneticisi : Prof.Dr. Ali Kara

Aralık 2019, 77 sayfa

Bu tez çalışmasında, Varyasyonel Kip Ayrıştırıcı (VKA) tabanlı Radyo Frekans (RF) parmak izi çıkarımı çalışılmıştır. RF parmak izi kullanımı, radyo cihazları tarafından iletilen geçiş(transient) sinyallerinin özniteliklerinin tanımlanmasına dayanmaktadır. RF cihazların geçiş sinyalleri, kısa süreli, durağan olmayan ve doğrusal olmayan zaman serileridir. Bundan dolayı, öncelikle VKA ile Bluetooth (BT) cihazların geçiş sinyalleri bant-sınırlı modlara ayrıştırılmakta ve ardından sinyal tekrar oluşturulmaktadır. Hem VKA ile yeniden oluşturulan hemde VKA modlarının yüksek dereceli istastiksel öznitelikleri çıkarılmaktadır. BT cihazlarını sınıflandırmada ise Doğrusal Destek Vektör Makinaları (DDVM-LSVM) sınıflandırıcısı kullanılmaktadır. Tez kapsamında önerilen yöntem, farklı marka, model ve seride BT cihazlarında deneysel olarak test edilmiştir. Önerilen VKA tabanlı RF parmak izi çıkarımı yönteminin, Hilbert-Huang transformu kullanılarak elde edilen zaman-frekans-enerji dağılımı tabanlı yöntemlerden en az %8 daha iyi bir başarım sağladığı deneysel veriler ile gösterilmektedir. Bu başarım, önceki yöntemdeki Sinyal-Gürültü Oranının (SGO-SNR) 2-3 dB altında ve daha az öznitelik ile elde edilebilmektedir. Ayrıca, VKA modlarının özniteliklerinin direk kullanılması durumundaki başarım, VKA ile yeniden oluşturulan sinyalden çıkarılan öznitelikler kullanılarek elde edilen başarımdan %4 daha yüksek bulunmuştur.

Anahtar Kelimeler: Varyasyonel Kip Ayrıştırıcı, Bluetooth Sinyalleri, Spesifik Emiter Kimliklendirme, Öznitelik Çıkarımı, Sınıflandırma.

To my family

ACKNOWLEDGMENTS

First, I give thanks to God for protection and ability to do work. I would like to express my special appreciation and thanks to my advisor Professor Dr. Ali Kara for his guidance, helpful advice and support, who made this work possible. His friendly guidance and expert advice have been invaluable throughout all stages of the work.

I would also like to thank my committee members, Prof. Dr. Bülent Tavlı and Asst. Prof. Gökhan Bakan for serving as my committee members even at hardship and for their time and valuable input. They have been a constant inspiration through their constructive criticism, insightful comments and patience.

Furthermore, my thanks are extended to the members of my examination committee.

Finally, I would like to thank my family for their support and encouragement.

TABLE OF CONTENTS

LIST OF TABLES

TABLES

LIST OF FIGURES

FIGURES

LIST OF SYMBOLS/ABBREVIATIONS

ADC	Analog-to-Digital Converter
ADMM	Alternate Direction Method of Multipliers
BPF	Band Pass Filter
BT	Bluetooth
CC	Correlation Coefficients
CM	Condition Monitoring
DHT	Discrete Hilbert Transform
EMD	Empirical Mode Decomposition
FH	Frequency Hopping
HHT	Hilbert-Huang Transform
HT	Hilbert Transform
IMFs	Intrinsic Mode Functions
IoT	Internet Of Things
IQR	Inter-Quartile Range
ITD	Intrinsic Time-scale Decomposition
LANs	Local Area Networks
LDA	Linear Discriminant Analysis
LSVM	Linear Support Vector Machine
PCA	Principal Component Analysis
PHY	Physical Layer
RFF	Radio Frequency Fingerprinting
RMSE	Root Mean Square Error
ROI	Region Of Interest
SNR	Signal-to-Noise Ratio
SS	Sums of Squares

STD	Standard Deviation
STFT	Short Time Fourier Transform
SVM	Support Vector Machine
TFA	Time–Frequency Analysis
VAR	Variance
VHF	Very High Frequency
VMD	Variational Mode Decomposition
WT	Wavelet Transform
WT	Wind Turbine
WV	Wigner Ville
WVD	Wigner-Vile Distribution

CHAPTER 1

INTRODUCTION

In the latest years, use of wireless communication systems has increased rapidly. The security of these systems has become more important recently. Therefore, wireless communication security should be improved. There are many software improvements, but these improvements are not enough for completely secure systems. Radio frequency fingerprinting (RFF) is one of the communication networks security techniques based on identification of the imperfections caused by a manufacturing process as unique features of the transceivers [1-3]. The work in [1], investigated the use of machine learning strategies to the classification and identification problem. In [2], a new RFF scheme using deep neural networks is presented. RFF of WiFi emitters were captures from energy spectrums of transient signals for device identification [3]. RFF systems consist of data collection, feature extraction and classification systems [4-7]. In [4], RFF is proposed to relieve essential user simulation attacks. This mitigation is skillful through low-end software-defined cognitive radio networks. A random noise waveform, combined with RF-DNA fingerprint used to identify antenna types and terminations [5]. In [6], deep learning used to find out physical layer attributes for the classification of cognitive radio transceivers. The applications of RFF technique lie in safe radio communications [8, 9], radar systems, military communications confrontation, civilian radio monitoring [10, 11], self-organized networks [12] and cognitive radio [13]. The RFF method is employed to improve the security of wireless communication networks, such as Wi-Fi networks, VHF radio networks and cellular networks. Phase, amplitude and frequency are the main elements for RF fingerprint process [14]. Statistical features such as variance, kurtosis and skewness are the features that can be extracted from these main elements of transient signal [15-17]. In [17], RF Fingerprint creation techniques for IoT devices depended on statistical characteristics are considered. Features can be obtained from different parts of the captured radio signals, such as turn-on transients, RF burst signals, preambles, etc.

RFF methods divided into two sets, namely transient based and modulation based RFF. Transient based technique extracts features from transient signals that exist at the beginning of the transmissions. Otherwise, modulation based techniques concentrate on modulator imperfections of the transceiver [18]. Many techniques have been used in time [19], spectral [20] and wavelet domain [15]. Recently many RFF techniques are introduced [21-23]. In [21], a multimodal method is proposed for improving RFF performance. [22], presents the groundwork for performing neural network-based (SEI) on IoT devices. [23], demonstrated a multi-sampling convolutional neural network for classifying ZigBee devices based on adaptive ROI selection. The importance of security for communication networks, prompted us to find out how can we develop and improve RFF as wireless networks security. When the emitting signals of wireless devices are noisy, it is difficult to distinguish the different wireless transmitters of these signals. Therefore we need to improve the signal processing functions on the captured signal before extracting the features. In this thesis, we propose to use variational mode decomposition (VMD) in RFF of Bluetooth signals. Radio transient signals are non stationary and non-linear time series. Extracting characteristic parameters of such transients in time domain will be necessary in classifying specific emitters, such as BT devices. However, classical techniques like Wigner-Vile distribution (WVD) and Wavelet techniques are hard to work with these transients since they are non stationary and nonlinear. For determining characteristic parameters of non stationary signals and classifying certain transmitter with high accuracy, a technique depends on EMD decomposition was proposed [24]. But the great disadvantages of EMD decomposition method are that it always associated with mode mixing problems [25, 26]. Also, EMD method suffers from computational complex. Lately, VMD decomposition method was suggested as new decomposition method [27]. VMD has the advantage that it is not associated with mode mixing problems and can operate in a simple computational manner. Therefore, to beat these issues, we employed VMD in RFF of Bluetooth signals. VMD is a new modal decomposition method, proposed in latest years as denoising method which is not used in the RFF of Bluetooth devices technique.

VMD is a very good robustness against the effect of background noise on the accuracy of signal decomposition and also, the VMD modes are a band limited functions which relieve the mixing issues [27-29].

In this thesis, VMD has been used for the first time in the RF fingerprint application of BT device classification by taking advantage of VMD to enhance identification performance and increase the accuracy of network security. The rest of this thesis is organized as follows: Chappter1 introduction. Chapter2 contains the brief introduction of variational mode decomposition. Chapter 3 Simulations included VMD decomposition and VMD parameters optimization. Chapter 4 RF fingerprint implementation included the transient signal decomposition using VMD, features extraction and BT devices identification using a linear support vector machine classifier, followed by conclusion in Chapter 5.

1.1. Background (Literature survey)

A naval technique was proposed to recognize various transceivers depended on the compression of sensing [30]. A large number of transmitted signals of wireless transceivers are very weak, long-range propagation and very similar to transient waveforms. Therefore, the complex analytic WT is employed to get the envelope of the transient signal and the identical properties are created by the compressed detection theory. Through a series of experiments, it was concluded that the proposed method effectively classifies received signals that are difficult to distinguish between their transient waveforms. A RF fingerprint algorithm with low sampling rates [31], is implemented, which is efficient at low sampling rates. It makes RF fingerprint reception more functional for mobile transmitters. To get the energy envelope of the processing signal, a Spectrogram using the SFT is applied and the unique properties of the envelope are extracted. The proposed algorithm was effectively used to identify a set of Bluetooth devices. The results demonstrate that the sampling rates are less effective on the accuracy of the suggested algorithm.

A new method for radar fingerprinting using unintentional modulation in radar signals is proposed in [32]. The suggested algorithm decomposes components into unconventional modulations using the Variational Mode Decomposition (VMD) technique. Then, the features that describe each component are calculated.

Simulations using real radar data demonstrate that the presented technique able to identify radar signals in the dataset with high performance.

A method for the appropriate classification of network devices in a wireless network is provided to detect jamming agents is presented in [33]. The method is depended on the analysis of the radio frequency (RF) fingerprinting of wireless network transceivers. On the preamble of RF fingerprinting, the signals transmitted by a wireless transmitters are repeatedly extractable and unique. Consequently, they can be used to classify the device as it is transmitted over the network. Recent studies show that this uniqueness exists, being referred to various sources: manufacturing, aging, environmental, etc.

Recent researches have shown that protection against attachment attacks can be done with a wireless physical layer device fingerprint [34].

Furthermore, fingerprint transceivers with cheap receivers have been notified to have conflicting accuracy, so radio frequency (RF) fingerprints often use high cost signal acquisition system. A strong RF fingerprint technique that is compatible with high-end and cheap receivers is presented.

The outcomes indicate that cheap radios may perform successful frequency fingerprint to detect fraud attacks on infrastructure networks. Traditional techniques like WVD and Wavelet techniques are hard to transact with non-stationary signals.

A new technique for the certain transmitter identity based on empirical mode decomposition (EMD) is presented to analyze the non-stationary signals [35]. This method achieves more efficient for implementing non-stationary characteristics and to classify certain transmitters with good accuracy. Based on the experiment results, it is demonstrated that the proposed method is effective for characteristic parameters of the transient signals to be better predicted from the wavelet.

The specific emitter identification approach depended on intrinsic time-scale decomposition (ITD) is suggested and investigated in [36], which represents an important improvement in transceivers definition, which is particularly helpful for the transient process. The ITD approach supplies a robust approach for real signals processing.

The technique can be employed in many applications such as Radar signals, wireless communications, voice and medical signal analysis.

A novel empirical mode separation technique in the recognition system of transceivers for wireless communication signals is described in [37]. The EMD approach is used in this system to separate signal modes, then component analysis (PCA) is applied to extract the certain characteristics. This system is successful for transient signals of low level of (SNR) and implements better than other techniques. The system is proficient in classifying certain emitters and can also be used for wireless communications security objectives.

Because of the conventional signal analysis process depended on FT is not appropriate method for non-stationary vibration signals of the hydropower and the limitation of the EMD decomposition technique, a new non-stationary and non-linear signal analysis approach" Analyzing of the hydropower vibration signals depend on VMD decomposition" is introduced in [38].

The simulation signals and actual signals are tested to measure the achievement of (VMD) decomposition method and (EMD) decomposition method. The results demonstrate that the VMD technique can prevent the mode mixing issue that appears in EMD decomposition method. The decomposed modes show good accuracy with the VMD method. Wind turbine (WT) condition monitoring (CM) signals usually include intra-wave properties that are hard to create by using traditional time–frequency analysis (TFA) since none of them is locally adaptable.

Intra-wave characteristics can be created only by EMD decomposition method and its expansion, but EMD method has some defects in TFA (Poor noise resistance, unknown fluctuations and low efficiency in detecting sideband frequencies). Superiorities of VMD decomposition with EMD decomposition in time–frequency characteristics creation and wind turbine condition monitoring is proposed in [25]. The experiment results demonstrated that VMD performance better than EMD method in noise resistance and also in multi-modes signal separation, side-band detection, and intra-wave characteristics creation.

1.2. Weakness of signal decomposition methods

1 - Empirical mode decomposition (EMD) disadvantages in signal decomposition and characteristics creation [26, 25]:

- Noise resistance: EMD approaches are very critical to signal noise. A slight change in the signal/noise ratio (SNR) of the signal can drive to notably various signal decomposition outcomes.
- Unknown fluctuations (ripples) are usually appears in the results achieved by EMD decomposition method, especially at low range of frequencies. They damage the characteristics of the signal and then make the signal difficult to interpret.
- Inactive in separating frequency components. Like the sideband properties produced by the fault, it cannot be effectively removed from the signal.
- The recursive calculations decrease the efficiency of calculation. Determination of upper and lower envelopes is one of the important steps in EMD and LMD computations. Then, the error introduced in the envelope computation is expanded to the decomposition outcoms.
- (IMF) generated by EMD decomposition method are not bandlimited functions. Therefore, EMD method is always correlated by mode mixing problems.

2- Two important parameters can affect VMD outcomes [39].

- Modes number (Z)
- Balancing parameter (α).

1.3. Problem statement

In recent years, the application of wireless communication systems has increased notably. The security of these systems has become more important day by day. For this reason wireless communication security should be developed.

Hardware of the transceivers has imperfections caused by a manufacturing process.

RF Fingerprinting is a technique based on identification of these imperfections as unique features of the transceivers. The importance of security for communication networks, prompted us to find out how can we develop and improve RFF as wireless networks security.

Through our study of several papers related to RFF in literature review, we find that (VMD) is a new modal decomposition method, proposed in latest years as denoising method which is not used in the RFF of Bluetooth devices technique. Due to the advantages of VMD and its modern, we have seen that it can be used in RFF technique to reduce the impact of noise on the transient signal of captured BT signal so increases the accuracy of features extraction and wireless networks security is improved. The performance of this method will be evaluated and compared with other existing methods.

VMD is a new decomposition method, proposed to decompose the signal into several discrete number of modes, and each mode is supposed to have compact frequency support around a central frequency.

VMD is an efficient in calculations, strong robustness against the effects of background noise and it's modes are narrow-banded functions, which relieves the mode mixing issues, and support the accurate extraction of features. For these reasons, VMD used as a part of our thesis proposal.

CHAPTER 2

VARIATIONAL MODE DECOMPOSITION (VMD)

Variational mode decomposition (VMD) is a decomposition technique [27]. The objective of VMD is to separate the input signal into different discrete modes u_z $(\mathrm{z} = 1,2,\ldots,\mathrm{Z})$, where Z is the number of the decomposed modes. Each discrete mode has limited bandwidth in the frequency domain, where each mode is supposed to be compacting around a center frequencyω_z $(\mathrm{z} = 1,2,\ldots,\mathrm{Z})$. The reconstructed signal is equal to the sum of the decomposition modes. VMD has a strong supporting mathematical theory, high operational efficiency and also has strong robustness against noise. VMD can deal well with non-stationary signals, since it does not suffer from mode mixing problem compared with other decomposition methods, such as wavelet and empirical mode decomposition [27]. The flow chart of VMD algorithm is shown in Fig (2.1).

2.1. Advantages and disadvantages of VMD

The objective of VMD is removing a noise or unwanted signals, thereby improving the quality and utility of the signals. When the signal contains random noise, a high frequency mode exists in the separated modes. If the high frequency modal component is removed, the random noise will be decreased [25, 26].

- VMD has a strong supporting mathematical theory, and also a high operational efficiency.
- VMD has good accuracy and stability in feature extraction, which can suppress the correlated noise.
- Has strong robustness against noise compared with other decomposition methods (wavelet decomposition and empirical mode decomposition)
- VMD is Non- recursive calculations, which increase the efficiency of decomposition calculation.
- Intrinsic mode functions of VMD are band-limited functions.

The disadvantage of VMD lies in predicting the values of the following parameters which may impact the accuracy of the VMD.

- Modes number (Z)
- Balancing parameter (α).

2.2. Construction and solution of optimization problem

VMD technique decomposes the given signal *f* into various components u_z known as modes using calculus of variation. The FT of each mode assumed to have compact support around the mean of the independent variable of the Fourier transform. This is otherwise known as the central frequency [27] and is denoted by ω_z.

The function of the VMD operation is to determine the spectrum of the modes and the central frequencies of these modes by optimizing the total addition of the bandwidth of the generated modes provided that the input signal is equal to the sum of modes. For this purpose, we construct an analytic function corresponding to the original mode by finding the Hilbert Transform of the mode u_z which in fact forms the conjugate harmonic of the mode u_z. Mainly, there are three stages for making each component: 1) transform the mode into complex signal.

2) the center frequency of mode shifted to zero frequency.

3) the shifted analytic signal should be smooth to determine the bandwidth of mode.

The separation procesure of signal f(t) is described as following.

The measure of bandwidth $\Delta\omega_z$ of each mode can be calculated by finding the integral of the square of the time derivative of the frequency-translated function component.

$$i.e.\,\Delta w_z = \int |\partial_t(u_z^D)|^2 \, dt \;\; = \|\partial_t(u_z^D)\|^2 \tag{2.1}$$

Therefore, the required minimization problem is

$$\min_{\{u_z\},\{\omega_z\}} \{\textstyle\sum_z \|\partial_t(u_z^D)\|^2\} \;\; , \quad s.t. \quad \textstyle\sum_z u = f \tag{2.2}$$

$$\min_{\{u_z\},\{\omega_z\}} \left\{\textstyle\sum_z \left\| \partial_t \left[\left(\delta(t) + \frac{j}{\pi t}\right) * u_z(t)\right] e^{-j\omega_z t}\right\|_2^2\right\} , \; s.t. \; \textstyle\sum_z u = f \tag{2.3}$$

To convert the minimization issu into non-constrained problem, the balancing factor α and Lagrangian multiplier λ are produced.

$$\mathrm{L}(\{u_z\},\{\omega_z\},\lambda) = \alpha \sum_z \left\| \partial_t \left[\left(\delta(t) + \frac{j}{\pi t}\right) * u_z(t) \right] e^{-j\omega_z t} \right\|_2^2 + \left\| f(t) - \sum_i u_i(t) + \frac{\lambda(t)}{2} \right\|_2^2 - \left\| \frac{\lambda(t)^2}{4} \right\|_2^2 \quad (2.4)$$

The non-constrained problem is minimized with respect to u_z , the minimization equation is rephrased as following:

$$u_z^{n+1} = \arg\min \left\{ \alpha \sum_z \left\| \partial_t \left[\left(\delta(t) + \frac{j}{\pi t}\right) * u_z(t) \right] e^{-j\omega_z t} \right\|_2^2 + \left\| f(t) - \sum_i u_i(t) + \frac{\lambda(t)}{2} \right\|_2^2 \right\} \quad (2.5)$$

This problem can be solved in spectral domain:

$$\hat{u}_z^{n+1} = \arg\min \left\{ \alpha \left\| j\omega \left[(1 + sgn(\omega + \omega_z)) \hat{u}_z(\omega + \omega_z) \right] \right\|_2^2 + \left\| \hat{f}(\omega) - \sum_i \hat{u}_i(\omega) + \frac{\hat{\lambda}(\omega)}{2} \right\|_2^2 \right\} \quad (2.6)$$

Change of variables $\omega \to \omega - \omega_z$ in the first term:

$$\hat{u}_z^{n+1} = \arg\min \left\{ \alpha \left\| j(\omega - \omega_z) \left[(1 + sgn(\omega)) \hat{u}_z(\omega) \right] \right\|_2^2 + \left\| \hat{f}(\omega) - \sum_i \hat{u}_i(\omega) + \frac{\hat{\lambda}(\omega)}{2} \right\|_2^2 \right\} \quad (2.7)$$

The two expressions are written as a space integral on the positive side frequencies:

$$\hat{u}_z^{n+1} = \arg\min \left\{ \int_0^\infty 4\alpha(\omega - \omega_z)^2 \left| \hat{u}_z(\omega) \right|^2 + 2 \left| \hat{f}(\omega) - \sum_i \hat{u}_i(\omega) + \frac{\hat{\lambda}(\omega)}{2} \right|^2 d\omega \right\} \quad (2.8)$$

The solution of this quadratic optimization problem is as following:

$$\hat{u}_z^{n+1}(\omega) = \frac{\hat{f}(\omega) - \sum_{i \neq z} \hat{u}_i(\omega) + \frac{\hat{\lambda}(\omega)}{2}}{1 + 2\alpha(\omega - \omega_z)^2} \quad , \quad (2.9)$$

The updating ceter frequency of each mode can be calculated as following:

$$\omega_z^{n+1} = \frac{\int_0^\infty \omega|\hat{u}_z(\omega)|^2 d\omega}{\int_0^\infty |\hat{u}_z(\omega)|^2 \, d\omega} \ , \tag{2.10}$$

The optimization procedure of VMD mainly includes the following steps [28]:

1) Initialize modes $\hat{u}_z^1$, ω_z^1 and $\hat{\lambda}^1$.

2) Update the modes $\hat{u}_z^{n+1}(\omega)$.

$$\hat{u}_z^{n+1}(\omega) = \frac{\hat{f}(\omega) - \sum_{i \neq z} \hat{u}_i^{n+1}(\omega) + \frac{\hat{\lambda}^n(\omega)}{2}}{1 + 2\alpha(\omega - \omega_z^n)^2} \tag{2.11}$$

3) This equation is for uppdatig the frequency ω_z^{n+1} .

$$\omega_z^{n+1} = \frac{\int_0^\infty \omega|\hat{u}_z^{n+1}(\omega)|^2 d\omega}{\int_0^\infty |\hat{u}_z^{n+1}(\omega)|^2 \, d\omega} \tag{2.12}$$

4) Update Lagrangian multiplier $\hat{\lambda}^{n+1}(\omega)$ to exact signal reconstruction until the convergence.

$$\hat{\lambda}^{n+1}(\omega) \leftarrow \hat{\lambda}^n(\omega) + \tau\left(\hat{f}(\omega) - \sum_z \hat{u}_z^{n+1}(\omega)\right) \tag{2.13}$$

$$\sum_z \|\hat{u}_z^{n+1} - \hat{u}_z^n\|_2^2 / \|\hat{u}_z^n\|_2^2 \quad < \varepsilon. \tag{2.14}$$

The VMD method suffers from the problem of not having a defined method for parameters selection that needs to be optimized to perform more accurate decomposition outcomes. Clearly, optimization of these parameters is very necessary for the implementation of VMD. The time step (τ), balancing parameter (α), the number of modes (Z), the tolerance of convergence (ε), and the initialization of center frequencies (ω_z^0), z=1,...., Z are the main parameters for VMD application.

Table. 2.1. VMD Main parameters and their functions.

Main parameters	Function of parameters	Possible adverse effects
Number of modes: Z	define the number of decomposed modes	too large Z will lead to redundant VMD information, while too small Z will lead to mode mixing in the VMD results
Quadratic penalty term: α	to encourage reconstruction quality: α is bandwidth control parameter of decomposed modes	reducing the bandwidth by increasing α may lead to capture the wrong centre frequency, too low an α makes the estimated modes contain more noise
Time-step of lagrangian multiplier: τ	to enforce constraints strictly: τ can ensure the exact reconstruction when the noise level of signal is low .	τ will become a strict impediment if the noise is high, and should be set to zero in this case

In our proposed method, the values of VMD input parameters namely ε, τ, ω_z^0, α, and Z, have been fixed to the values 10^{-7} , 0, 0, 200 and 3, respectively [27, 29, 39]. The main parameters and their functions are concluded in Table 2.1.

2.3. Evaluation criteria for denising algorithms

One of the most widely used metrics is the (signal/noise) ratio SNR. The terms signal and noise actually come from radio engineering, in which a signal is the noise-free signal and noise is the white noise. Signal processing is the statistical technique used to extract information from the raw signal. To determine the strength of a signal, the so-called (signal/noise) ratio SNR must be calculated. For the high ratio SNR means that the true signal is much greater than the noise and can be easy to capture useful characteristics from the raw signal. So, it is known as the ratio of signal power to the ratio of noise power.

This ratio has many important applications in applied mathematics, analytical chemistry, electronics, and the geosciences.

In electronics, signal and noise are measured in decibels. There are various ways in which noise performance can be estimated. If the original signal is known, the most popular approach (signal / noise) ratio or SNR is to measure the strength of the signal relative to the nose. Of course, the greater the variance between the original signal and the undesirable noise, gives the higher the S/N ratio or (SNR), the better measuring performance. The signal to noise ratio refers to the ratio of the original signal to the undesirable background noise.

$$SNR = \frac{P_{signal}}{P_{noise}} \tag{2.15}$$

Usually a (signal/noise ratio) formed in a logarithmic basis using (decibels) [40, 41]:

$$SNR_{dB} = 10 \log_{10}\left(\frac{P_{signal}}{P_{noise}}\right) \tag{2.16}$$

$$SNR_{dB} = 10 \log_{10}\left(\frac{\|f\|}{\|\hat{f}-f\|}\right) \tag{2.17}$$

$$\|f\| = \left(\sum_{i=1}^{M}|f_i|^2\right)^{\frac{1}{2}} \tag{2.18}$$

If the levels are measured in decibels, the equation can be written as:

$$SNR_{dB} = (P_{signal})_{dB} - (P_{noise})_{dB} \tag{2.19}$$

Another statistical parameter method measures the error between two values. Otherwise, it makes a comparison between the expected value and the known value. This method is called Root Mean Square Error (RMSE) and also called as Root Mean Square Deviation. This is one of the most well-known methods using statistical parameters.

$$RMSE = \sqrt{\frac{\|\hat{f}-f\|^2}{M}} \tag{2.20}$$

$\|.\|$. Two norm is a function which assigns real number called norm.

Where $\hat{f}$ is the original signal and M is the signal length. The (signal / noise) ratio SNR and root mean square error (RMSE) are predictive measures for signal strength measurement, respectively.

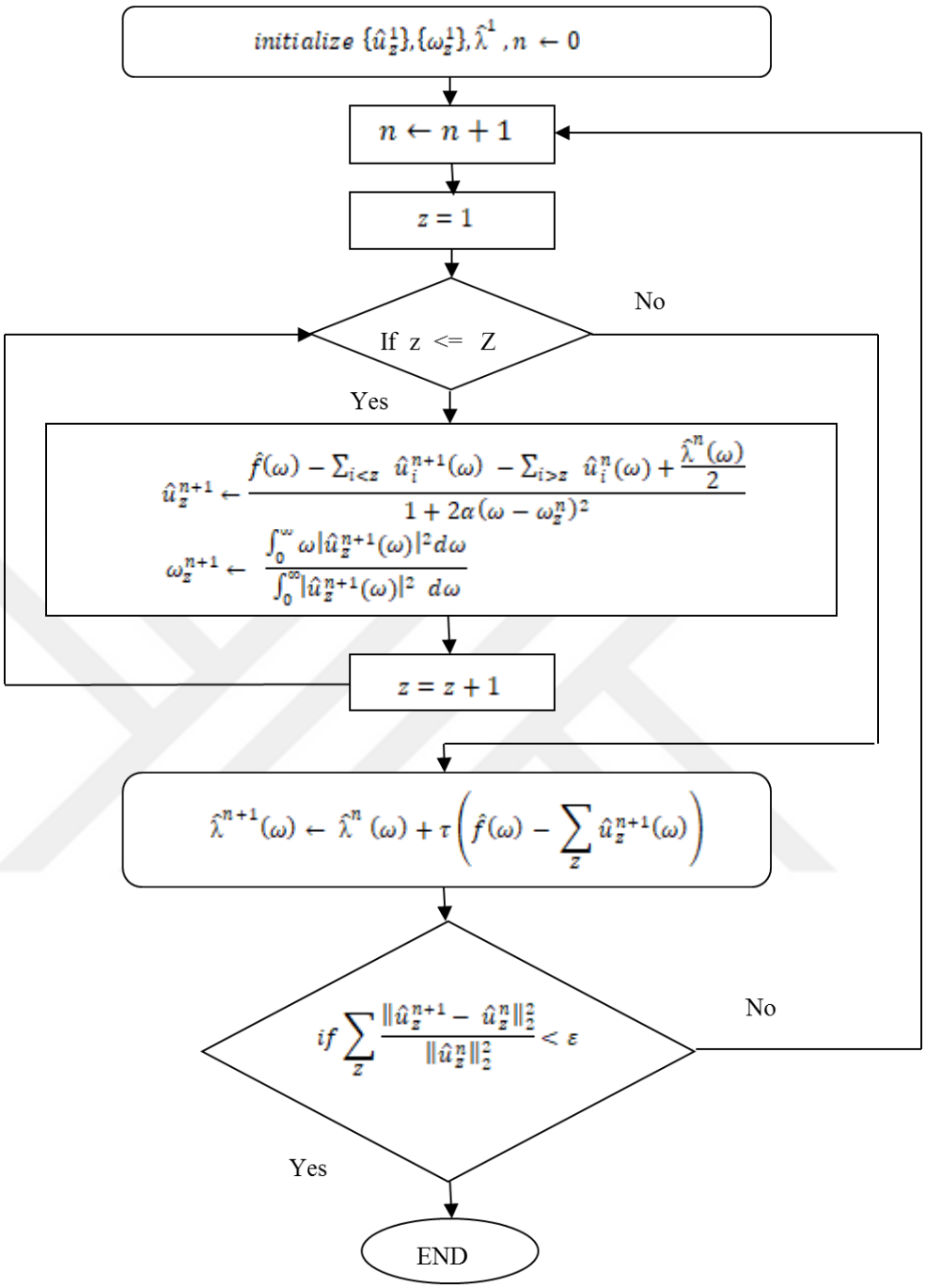

Figure 2.1 Flow chart of VMD algorithm

CHAPTER 3

VMD SIMULATIONS

3.1. Noise robustness

In this section we applied the variational mode decomposition method (VMD) on some synthetic simulation signals, which are consisted of three harmonics superimposed Gaussian white nose $\eta(t)$, to test the noise robustness and the affect of number of components Z. A simulation signal f (t) is prepared to evaluate noise robustness using the VMD technique.

$$f(t) = \cos(2\pi f_1 t) + \frac{1}{4}\cos(2\pi f_2 t) + \frac{1}{16}\cos(2\pi f_3 t) + \eta(t), \qquad (3.1)$$

Where the frequency of components are:

f_1 = 2; f_2= 24; f_3= 288;

And the noise level is $\sigma = 0.1$, where σ is standard deviation. This value is suitable with respect to the amplitude of the signal components. Since our goal is not the exact reconstruction signal, To eliminate noise, we apply variational mode decomposition technique to the simulation signal without the Lagrangian multiplier.

The three recovered modes performed by VMD are shown in the Fig. 3.1. The strongest mode with lowest frequency is reconstructed clearly with (SNRo =35dB). The medium- strength signal is recovered with (SNRo =17dB). The weak, high frequency mode is affected by the noise but the component frequency is captured correctly (SNRo =5dB).

Increasing the value of α will decrease the band width, which may causes the problem of not catching the exact center frequency, while the wide band width resulted by using too small α leads to noisy recovered modes [27,25].

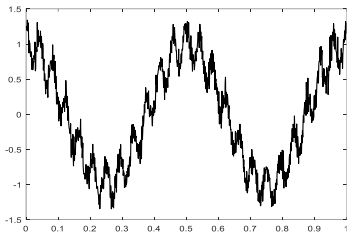

(a) f(t)

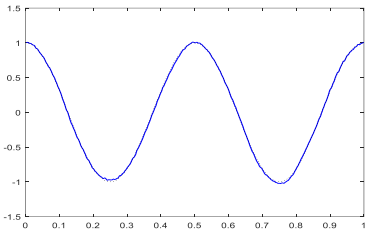

(b) u_1 (t), SNRo =35dB

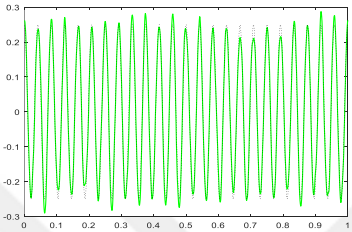

(c) u_2 (t), SNRo= 15dB

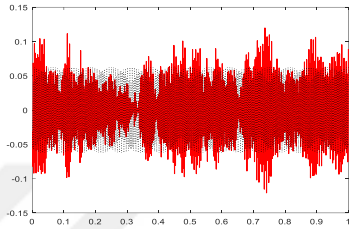

(d) u_3 (t), SNRo = 5dB

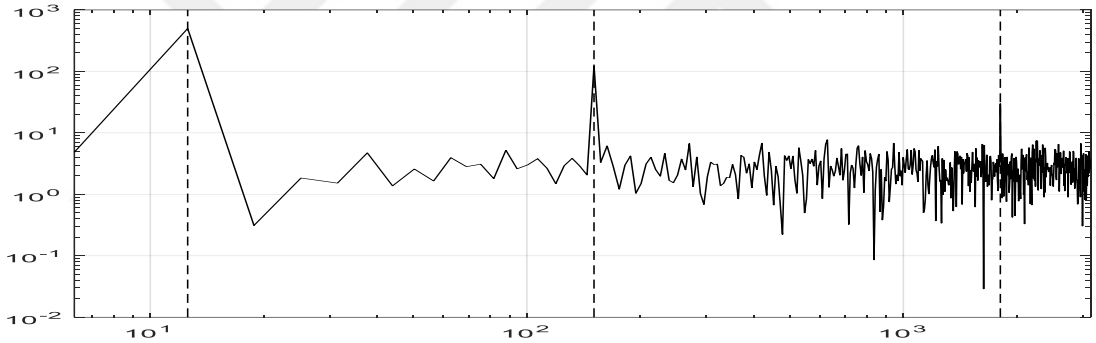

(e) $|\hat{f}|(\omega)$

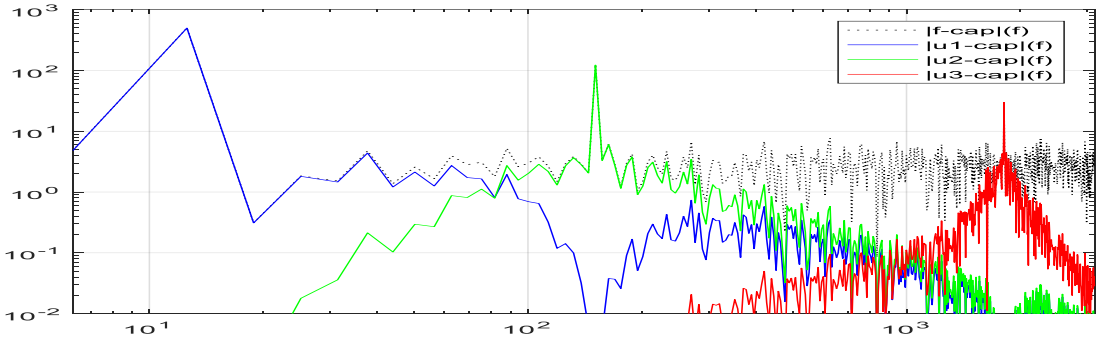

(f) $|\hat{u}_z|(\omega)$

Fig.3.1. Noisy signal decomposition. (a) Input signal. (b) (c) (d) Reconstructed modes (e) Input signal spectrum and mode- frequencies. (f) Spectrum of modes.

3.2. Segmentation

The classic weakness of many segmentation algorithms is how many clusters (or modes in the current state) must be specified to mark pre-segmentation. This is the same shortcoming with VMD. The number of modes Z is very important parameter in the signal decomposition by VMD [27].

Z Should be defined in advance to tell how many modes in the present signal. Here we are going to examine the effects of over- and under-segmentation of the given data, where under-segmentation is too few modes and over- segmentation is too many modes. We estimate here the results of VMD using too few or too many modes, using the input signal given in (3.1). For this study, we use a tri-harmonics signal, however at small noise level of $\sigma = 0.005$. We perform VMD with Z=2 (under-segmentation, too few modes) and Z=4 (over-segmentation, a large number of modes). The decomposition results also depend on the bandwidth which is introduced by balancing factor (α) as illustrated in Fig.3.2, the decomposition results are shown as following:

For under-segmentation (Z=2), there will be sharing between the neighboring modes for small alpha (α=100), or mostly discarded modes for big alpha ($\alpha = 10000$ and no Lagrangian multipliers).

On the other hand, when over-segmentation (Z=4), and small band width control parameter ($\alpha = 100$), one or several modes get noisy and broad spectral density. For large value of (α =10000), the center frequency of two or more modes get matched (mode duplication) and some of important parts of signal spectrum shared with others.

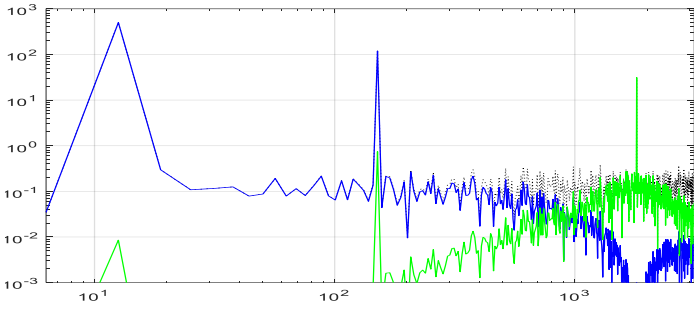

(a) $|\hat{u}_z|(\omega)$, Z=2, $\alpha = 100$

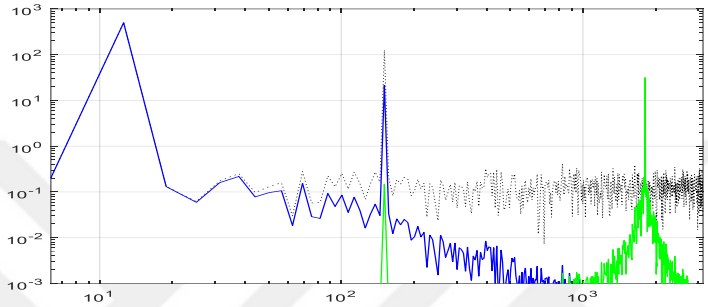

(b) $|\hat{u}_z|(\omega)$, Z=2, $\alpha = 10000$

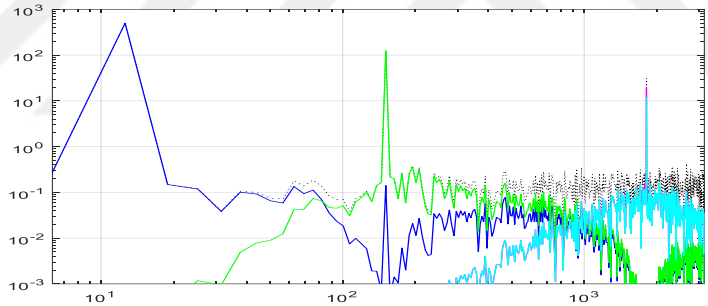

(c) $|\hat{u}_z|(\omega)$, Z=4, $\alpha = 100$

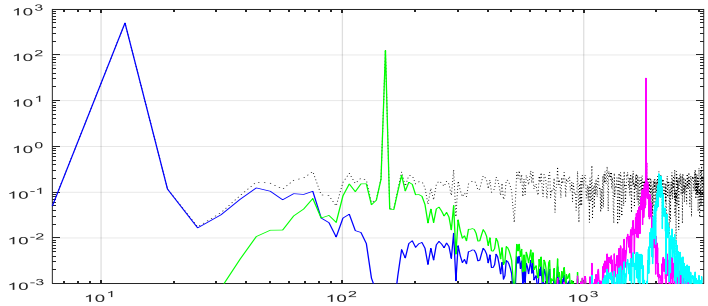

(d) $|\hat{u}_z|(\omega)$, Z=4, $\alpha = 10000$

Fig. 3.2 Number of modes influence. (a), (b) small number of modes. Some modes are contained in other modes (smallα) or discard (bigα). (c), (d) large number of modes either get more noise (small α), or mode duplication (bigα).

3.3. Optimization of the number of modes Z

The number of modes Z must be predefined prior the VMD computation starts. Theoretically, the value of Z depends on how many components are present in the signal. When the value of Z is improperly realized, the unneeded computations are increased, and at the same time the accuracy of signal separation may be affected [27]. Redundancy VMD information is caused when too many modes are selected and mode mixing results in VMD will appear for too few modes. Therefore, it is very important to find the optimal value of Z to get high accuracy and efficient computation of the VMD. However, traditional VMD can't perform such an optimization. However, traditional VMD can't perform such an optimization. The question of how to find the optimal value of Z has not yet been answered, but it remains to solve. The determination of Z depends on the experience of the researchers. In this study, we assume that the number of mode functions (Z) is equal to the number of modes (IMF) generated by empirical mode decomposition [42], followed by the decomposition method (VMD) jointed with correlated coefficients (CC). Firstly, the simulation signal is decomposed into discrete number of mode functions equal to the same number of mode functions that decomposed by EMD method; the correlation coefficients between the input simulation signal and the generated intrinsic mode functions are computed and based on selected threshold value, we determine the useful CCs and discard the noisy mode functions (IMFs).

3.3.1 Correlation coefficients

The relationship between the two variables can be measured by correlation coefficients (CCs) [42]. The CCs are values ranging from (-1) to (1). If the relationship between the variables is completely positive linear, CC is 1, but if the relationship is negatively related, CC is -1. The correlation coefficient is 0 when the relationship between the variables is not linear. There are two kinds of correlation coefficients; one of them is Spearman's rank correlation coefficient, which is depends on the rank association between the amounts. The second technique is the most popular technique for measuring the relationship between two quantities which is called Pearson's correlation coefficient.

3.3.2 Pearson's correlation coefficient

Pearson's correlation coefficient (r), sometimes referred to as the correlation coefficient or r, is the most popular technique used to optimize the relationship between two quantities in which this relationship is positively correlated, negatively correlated or nonlinear relationship (not a straight line).

The r values of the two elements are frequently reported in research articles and journals, to summarize the relationship between two elements.

The value r will be positive and much greater than zero, when the two quantities have a linear straight line relationship in the positive direction. The value r is less than 0, when the relationship is straight line in negative. When the values of (r) are very close to zero then the relationship between the two quantities is small. The range of values (r) is from -1 to 1.

To calculate Pearson's correlation coefficient (r), assumed that we have two quantities u and v [43].

$$r = \frac{SS_{uv}}{\sqrt{(SS_{uu})(SS_{vv})}} = \frac{\sum_{i=1}^{N}(u_i-\bar{u})(v_i-\bar{v})}{\sqrt{\sum_{i=1}^{N}(u_i-\bar{u})^2 \sum_{i=1}^{N}(v_i-\bar{v})^2}} \quad (3.2)$$

In order to find the correlation coefficient of two quantities, we usually need three additions. The squares sum of the quantity (u), squares sum of the quantity (v) and the cross product sum of (uv)

Let the mean of u be

$$\bar{u} = \frac{1}{N}\sum_{i=1}^{N} u_i \quad (3.3)$$

And the mean of v

$$\bar{v} = \frac{1}{N}\sum_{i=1}^{N} v_i \quad (3.4)$$

The squares sum of quantity (u) is

$$SS_{uu} = \sum_{i=1}^{N}(u_i - \bar{u})^2 \quad (3.5)$$

The squares sum of quantity (v) is

$$SS_{vv} = \sum_{i=1}^{N}(v_i - \bar{v})^2 \quad (3.6)$$

The cross-products (*SS*uv) sum

$$SS_{uv} = \sum_{i=1}^{N}(u_i - \bar{u})\,(v_i - \bar{v}) \tag{3.7}$$

The correlation coefficient's sign indicates whether the correlation is greater than zero (positive) or less (negative).

(r) = −1, this value indicates that the correlation is negative with all (u, v) and is in a straight line with negative gradient;

(r) = 1, this value indicates that the correlation is positive with all (u, v) and is in a straight line with positive gradient;

(r) = 0 this value indicates that the relationship between the two quantities is not linear. The relationship strength between the variables is estimated by the magnitude of the correlation coefficient [43]:

$0 < |r| < .3$ weak correlation

$.3 < |r| < .7$ moderate correlation

$|r| > 0.7$ strong correlation

3.4 Influence of α parameter on VMD performance

Alpha (α) is a balancing parameter to encourage reconstruction quality. That sometimes called frequency bandwidth control parameter, which significantly affect the VMD results. When the value of balancing parameter α is small, the frequency bandwidth becomes wide, and the opposite is true [27].

When the bandwidth is wide, more noise and unwanted frequencies are involved in the denoising result. Then, the signal/noise ratio (SNR) of the denoising results will be reduced and will increase the rigidity of the signal interpretation. Moreover, the very large balancing parameter α, which controls the bandwidth, can produce very narrow frequency bandwidth and causes the problem that some parts of the signal are discarded when the number of modes is too small. However, a large number of modes will cause a sharing between the adjacent modes of the same frequency.

As a summary, increasing the value of α parameter results in a reduction in bandwidth and is difficult to capture the correct central frequency, but when the α value is too small it contains more noise in the predicted mode.

Therefore, to obtain the accuracy of the VMD decomposition, the α parameter, that is, known as frequency bandwidth control, must be optimized in the implementation of VMD

3.5. Simulations

To minimize the number of modes, we used a combination of VMD and correlation coefficient (CC). To separate the simulation signals into intrinsic mode functions (IMFs) and define noise mode functions and useful mode functions, respectively; the number of modes in VMD is selected to be equal to the number of modes by empirical mode decomposition(EMD) as a default [42]. The distinction between noise mode functions (IMFs) and useful mode functions (IMFs) can be made according to the threshold of the (CCs). Then, the reconstructed signal is performed by adding the useful IMFs.

To measure the performance of variational mode decomposition (VMD) denoising algorithm, simulation experiments have been carried out in this section, with different input SNRs were used in the range from −10 dB to 5 dB. The formula of correlation coefficient (CC), as statistical parameter is shown as following:

$$r = \frac{\sum(f-\bar{f})(u_z-\bar{u}_z)}{\sqrt{\sum(f-\bar{f})^2 \sum(u_z-\bar{u}_z)^2}} \tag{3.8}$$

Where f is a simulation signal and u_z is mode components of VMD.

3.5.1 Simulation 1

The objective of this simulation is to optimize the number of decomposition modes Z, by CCs and measure the performance of different input SNRs.

The simulation signal $x(t)$ is consisting of three components of the frequencies,

f_1 =10, $f_2 = 50$, $f_3 = 100$.

Where the noisy signal$f(t)$ is a mixing of the simulation signal $x(t)$ and the Gaussian white noise $\eta(t)$ with noise level $\sigma = 0.5$.

$$f(t) = 0.8\cos(2\pi f_1 t) + 0.6\cos(2\pi f_2 t) + 0.3\cos(2\pi f_3 t) + \eta(t), \tag{3.9}$$

The waveform of noisy signal in time domain is illustrated in Figure 3.3.

The decomposition modes and denoising results of VMD for a noisy signal is presented in Figure 3.4 and Figure 3.5 respectively, where the number of IMFs by VMD is set to Z=9, which is equal to the number of EMD and $\alpha = 7000$. As seen in Figure 3.5, the reconstructed signal of VMD is improved after we make denoising, where the input SNRi =3 dB and the resultant SNRo=15.6 dB.

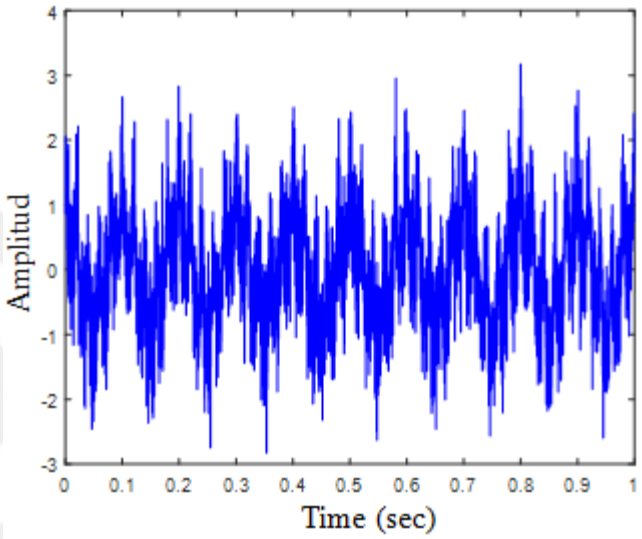

Figure 3.3 The waveform of noisy signal in time domain (SNRi=3dB).

The correlation coefficients (CCs) between the mode functions (IMFs) and the input noisy signal are recorded in Table 3.1, According to selected threshold which is 0.24. We get three useful IMFs by VMD.

Table 3.1 (CCs) Calculations between VMD (IMFs) and noisy signal.

IMFs	IMF1	IMF2	IMF3	IMF4	IMF5	IMF6	IMF7	IMF8	IMF9
CCs	**0.626**	**0.480**	**0.252**	0.152	0.147	0.156	0.165	0.175	0.195

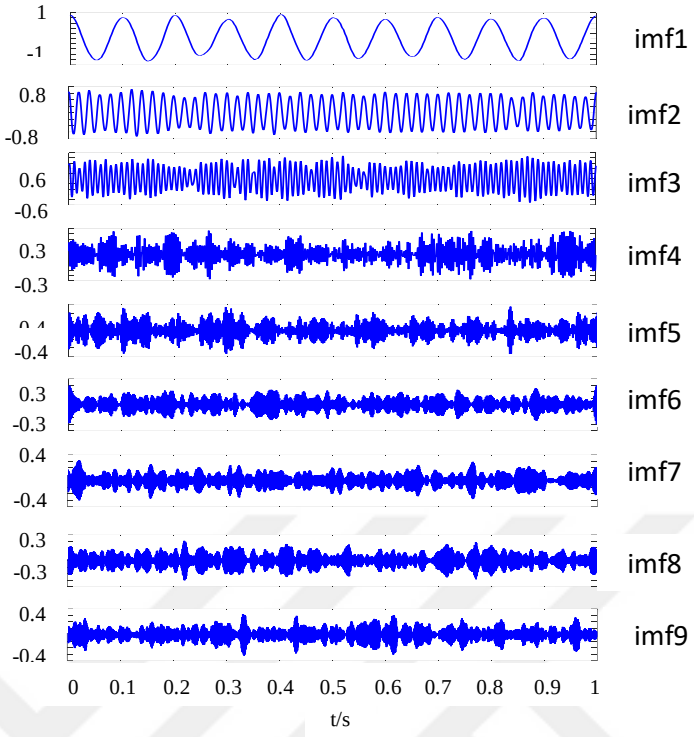

Figure 3.4 The IMFs of noisy signal;

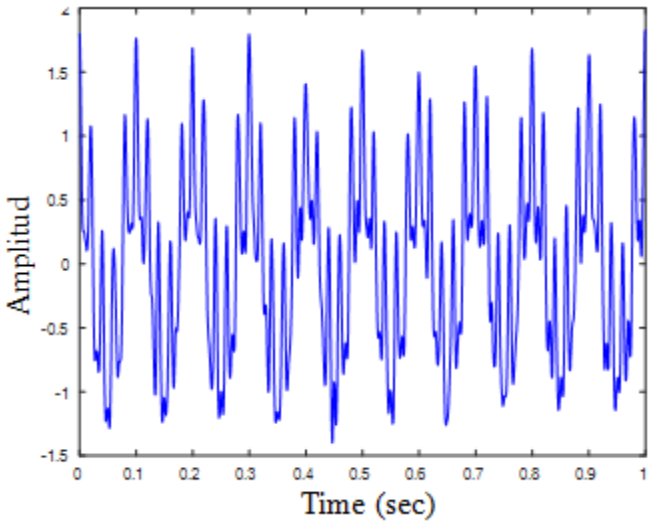

Figure 3.5 Time-domain denoising signal (15.6dB).

To measure the achievement of VMD with respect to various input (SNRs) ranging from -10 dB to 5 dB [42], the output SNRs and RMSE are recorded in Table 3.2, and Figure 3.6 illustrates the plots of input SNRs versus output SNRs for simulation signal. The relation between input SNRi and output SNRo is proportional, when the input SNRi increases the output SNRo increases too and RMSE decreases.

Table 3.2 Denoising results of noisy signal with different SNRs.

σ	2.4	2.1	1.7	1.3	1.06	0.85	0.65	0.53	0.41
SNRi	-10.4	-9.1	-7. 3	-4.9	-3.06	-1.06	1.17	2.79	5.16
SNRo	-0.68	0.20	2.62	5.17	7.66	10.71	13.12	14.64	17.89
RMSE	0.80	0.73	0.51	0.37	0.31	0.20	0.15	0.12	0.10

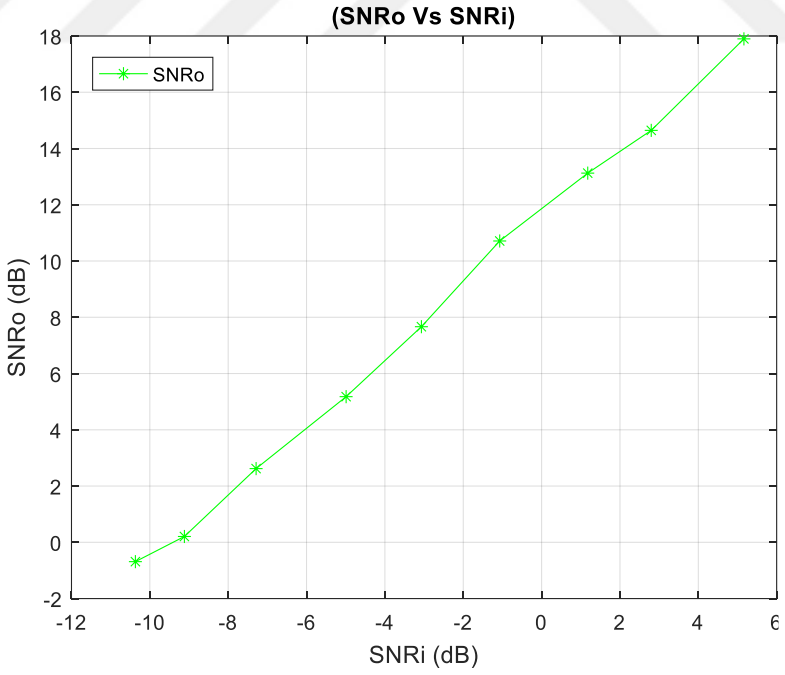

Figure 3.6 Denoising results of noisy signal with different SNRs.

3.5.2 Simulation 2

The objective of this simulation is to measure the influence of α on the denoising results. Considering a noiseless signal $x(t)$ is mixed by an additive noise $\eta(t)$.

In which $\eta(t)$ is white Gaussian noise with noise level $\sigma = 0.5$.

$$f_1 = 10, \qquad f_2 = 50\,, \qquad f_3 = 100.$$

$$f(t) = 0.8\cos(2\pi f_1 t) + 0.6\cos(2\pi f_2 t) + 0.3\cos(2\pi f_3 t) + \eta(t) \qquad (3.10)$$

We apply the VMD to the noisy signal with Z=3, and different values of band width control parameter α, to measure the effect of α parameter on the reconstruction signal. Signal to nose ratio SNR can be employed to measure the performance of different balancing parameters α.

The output SNRs and α are listed in Table 3.3, and Figure 3.7, shows the plots of α versus output SNRs for simulation signal. Output SNRo of denoised signal is increasing with increasing of (α) parameter and the relation between input SNRi and output SNRo is proportional, for high SNRi we have high SNRo.

Table 3.3 Denoising results of noisy signal with different α .

SNRi	SNRo				
	α = 1000	α = 6000	α =11000	α =16000	α =21000
-10.0	-4.90	-0.99	0.78	2.07	3.16
-9.17	-3.88	-0.24	2.07	2.63	3.01
-7.40	-1.92	1.93	4.14	5.00	5.34
-4.78	0.74	5.52	7.64	8.14	8.47
-3.16	2.35	7.06	9.35	9.76	10.06
-1.72	3.82	8.47	10.59	11.09	11.44
-1.26	4.23	8.74	10.70	11.13	11.44
0.38	5.91	12.00	12.68	13.09	13.38
1.10	6.62	13.03	13.83	14.30	14.64
1.78	7.37	13.47	14.16	14.58	14.89
2.88	9.65	14.58	15.26	15.68	15.99
4.16	10.79	15.85	16.56	16.98	17.29
5.00	11.78	16.32	16.96	17.35	17.62

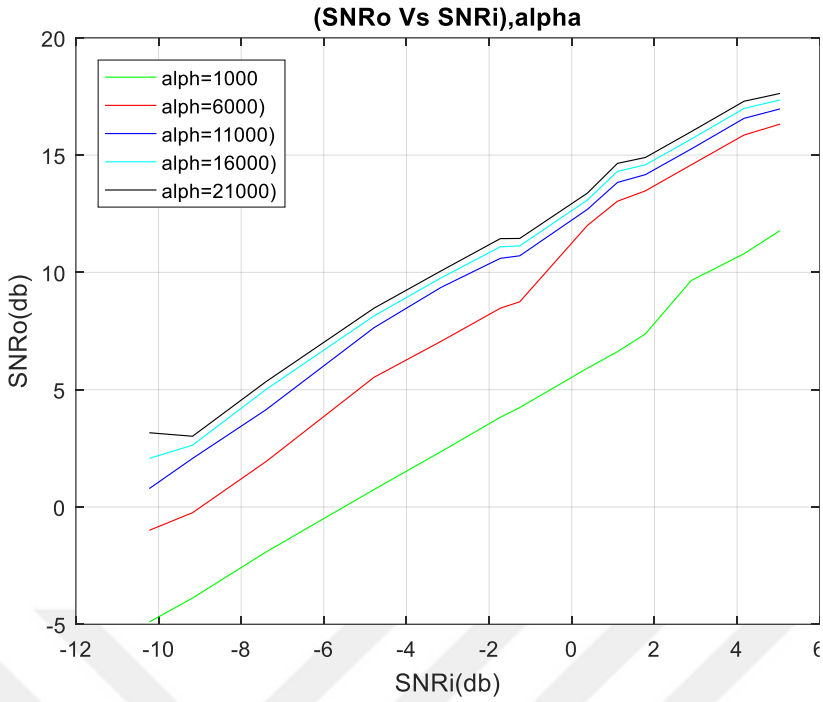

Figure 3.7 Denoising results of noisy signal with different α .

3.6. Decomposition of complex multimode signals

In this section we considered some of slightly more complex signals to be decomposed. The objective of this simulation part is to apply VMD on wide band signals. Examples of complex signals: piecewise stationary signals, general trend signals, general quadratic trend signals, chirp signals.

3.6.1 Decomposition of piecewise-stationary signals

In this example we considered the Piecewise stationary signal as follows:

$$f(t) = \cos(120\pi t\ )\, I(0 \le t \le 0.5) + \cos(\ 80\pi t)\, I(0.5 \le t \le 1), \qquad (3.11)$$

This signal is non stationary over the time range $(0 \le t \le 1)$ but is stationary on $(0 \le t \le 0.5)$ and $(0.5 \le t \le 1)$ respectively. The piecewise signal has spectral peaks at 120π and 80π. VMD results are illustrated in Figure 3.8. The central frequencies of reconstructed modes converge to the assumption frequencies and the time domain modes show good separation [27].

3.6.2 Decomposition of chirp signal

$$f(t) = \cos(5\pi t + 70\pi t^2), \quad 0 \le t \le 1 \tag{3.12}$$

For t ∈ [0, 1] the instantaneous frequency varies linearly between 5π and 145π. We chose to decompose the signal into three modes [27]. The captured center frequencies ω_k converge to the expected frequencies properly, and the recovered modes were nicely separated. Figure 3.9 shows the results of VMD decomposition.

3.6.3 Decomposition of general linear trend signal

This signal is a combination of three components, a linear trend and two different harmonics [25]:

$$f(t) = 6t + cos(8\pi t) + 0.5\cos(40\pi t)\,,\ 0 \le t \le 1. \tag{3.13}$$

VMD results are illustrated in detail in Figure 3.10. From the figure we can see how the two non-zero center frequencies ω_2 and ω_3 converge towards the exact harmonics. The corresponding modes form a nice section of the input spectrum, with each mode clearly placed around its corresponding center frequency. In the time domain, the three reconstruction modes are very clearly and beautifully separated.

3.6.4 Decomposition of general quadratic trend with chirp and piecewise signal

This signal composite of three components, a quadratic trend, chirp signal and piecewise stationary signals [25].

$$f(t) = 6t^2 + \cos(10\pi t + 10\pi t^2) + \cos(60\pi t\ )\, I(0 \le t \le 0.5) + \cos(\ 80\pi t - 10\pi)\, I(0.5 \le t \le 1) \tag{3.14}$$

Thus, for t ∈ [0, 1] the instantaneous frequency varies linearly between 10π and 30π. So, the spectrum of the chirp mode is placed at the peak of 20π. The expected spectral peaks of the piecewise components are at 60π and 80π. VMD results are illustrated in Figure 3.11. The computed center frequencies ω_z converge exactly the predicted frequencies. The input signal is decomposed into four modes; therefore the piecewise signal is presented as two separate modes. The spectral plot of different modes, show that the spectral separation is nicely estimated.

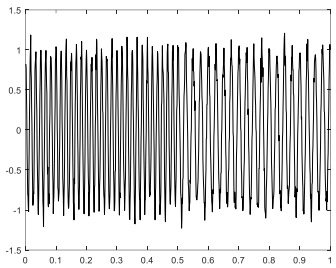

(a) f(t)

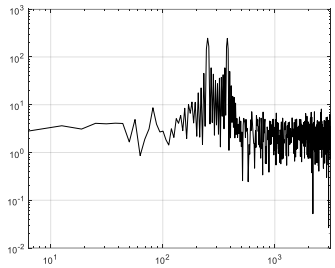

(b) $|\hat{f}|(\omega)$

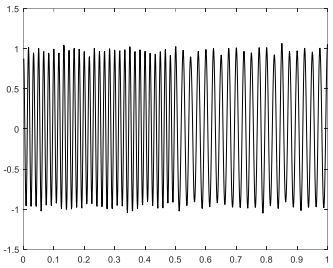

(c) Reconstructed signal

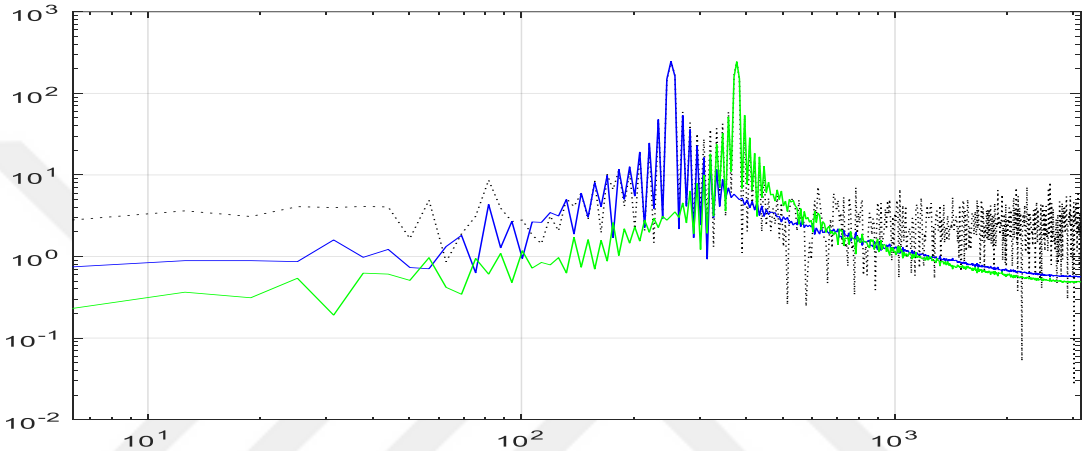

(d) $|\hat{u}_z|(\omega)$

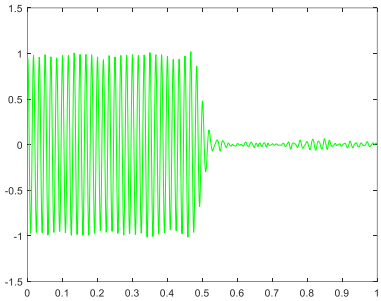

(e) $u_1(t)$

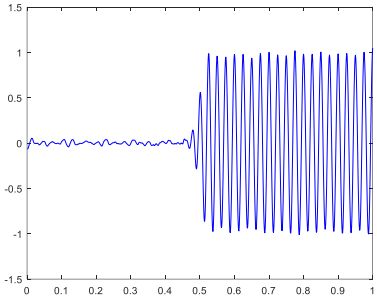

(f) $u_2(t)$

Fig 3.8 VMD decomposition of f(t) . (a) Input signal f(t). (b) The signal's spectrum. (c) VMD reconstructed signal. (d) VMD's spectral decomposition. (e)–(f) Reconstructed modes.

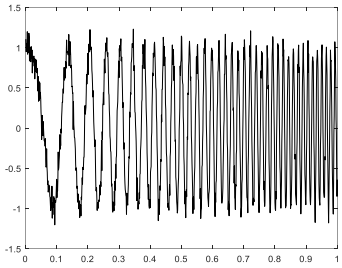

(a) f(t)

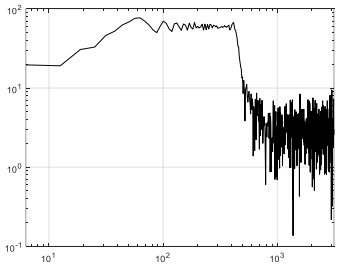

(b) $|\hat{f}|(\omega)$

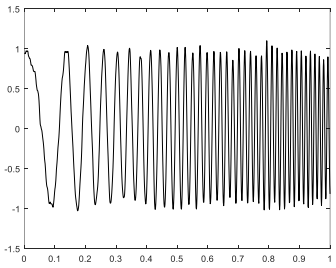

(c) Reconstructed signal

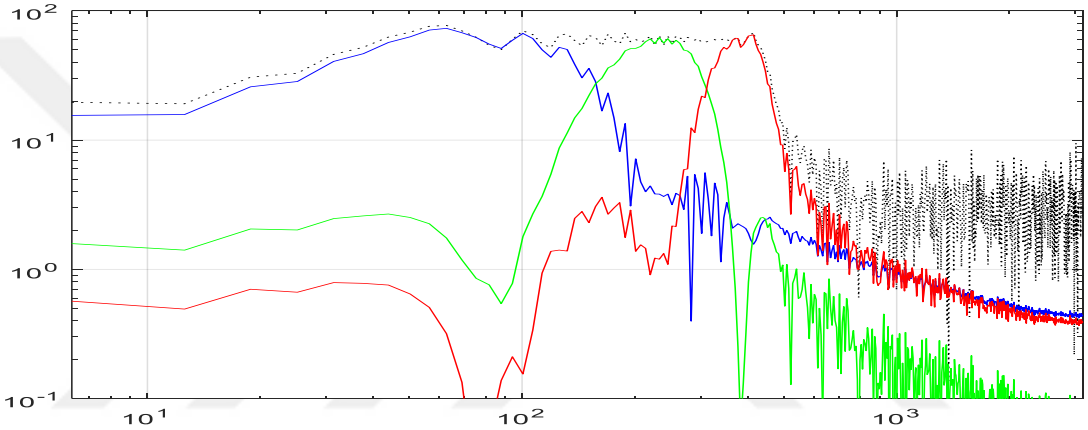

(d) $|\hat{u}_z|(\omega)$

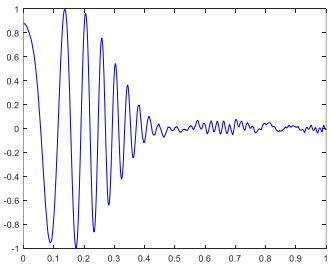

(e) $u_1(t)$

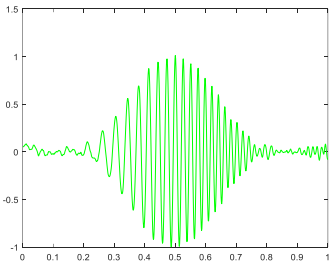

(f) $u_2(t)$,

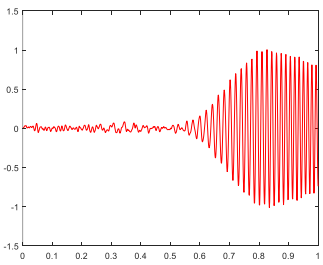

(g) $u_3(t)$

Fig 3.9 VMD decomposition of f(t) . (a) Input signal f(t). (b) The signal's spectrum. (c) VMD reconstructed signal. (d) VMD's spectral decomposition. (e)–(g) Reconstructed modes.

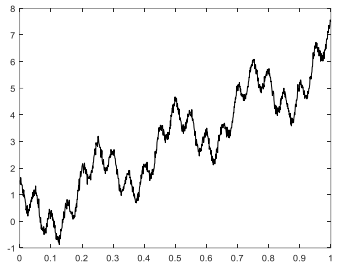

(a) f(t)

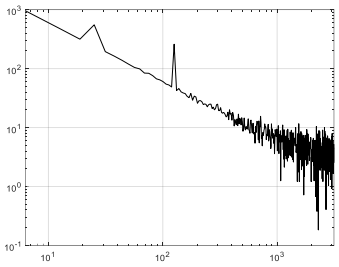

(b) $|\hat{f}|(\omega)$

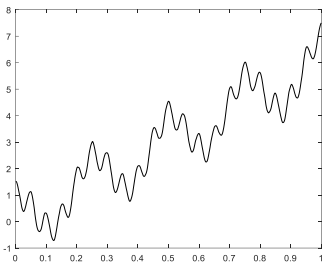

(c) Reconstructed signal

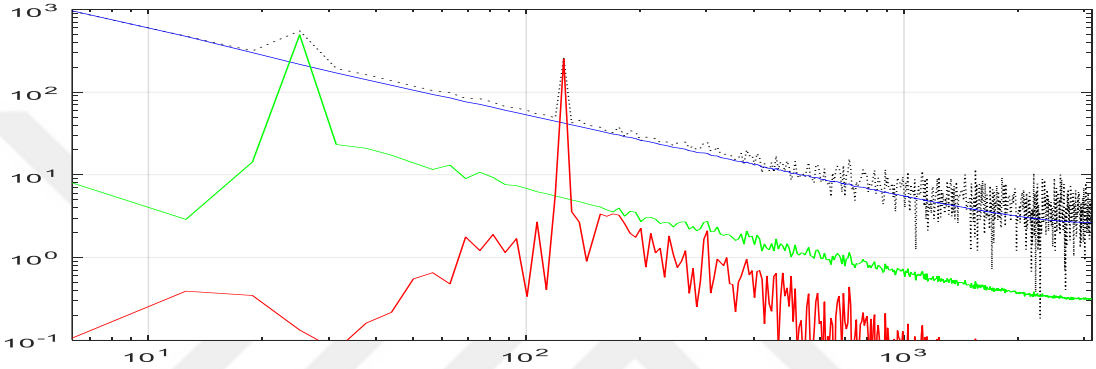

(d) $|\hat{u}_z|(\omega)$

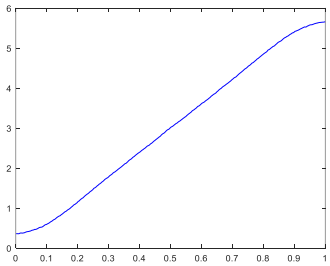

(e) $u_1(t)$

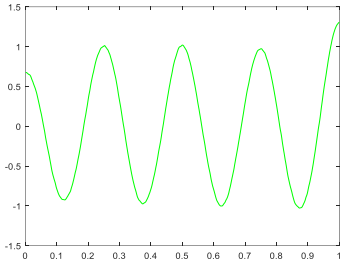

(f) $u_2(t)$

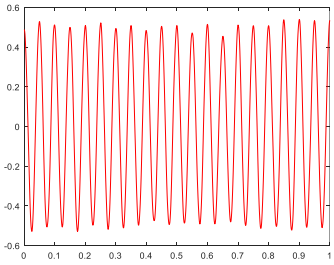

(g) $u_3(t)$

Fig. 3.10. VMD decomposition of f(t) . (a) Input signal f(t). (b) The signal's spectrum. (c) Reconstructed signal. (d) VMD's spectral decomposition. (e)–(g) Reconstructed modes

.

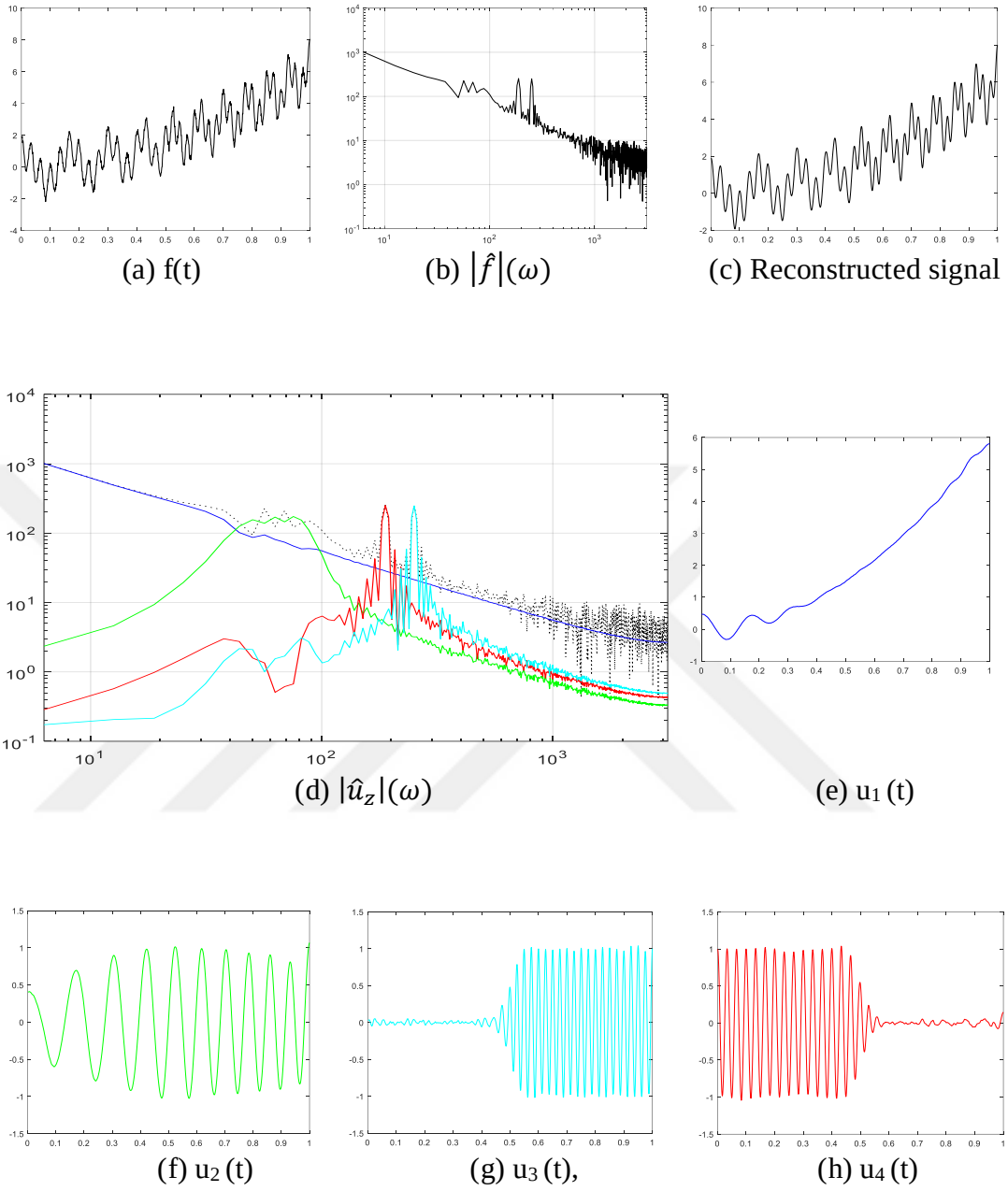

(a) f(t) (b) $|\hat{f}|(\omega)$ (c) Reconstructed signal

(d) $|\hat{u}_z|(\omega)$ (e) u_1 (t)

(f) u_2 (t) (g) u_3 (t), (h) u_4 (t)

Fig 3.11 VMD decomposition of f(t) . (a) Input signal f(t). (b) The signal's spectrum. (c) Reconstructed signal. (d) VMD's spectral decomposition. (e)–(h) Reconstructed modes.

CHAPTER 4

VMD BASED RF FINGERPRINT AND RESULTS

RF fingerprinting is a technique prepared to catch the unique features of the RF energy of the emitting devices, to identify mobile phones and other transceivers. The RF fingerprinting system Fig.4.1 is designed to identify set of Bluetooth signals emitted from a set of mobile phone devices. The carrier frequency bandwidth of the Bluetooth signal ranges from 2400 MHz to 2483.5 MHz.

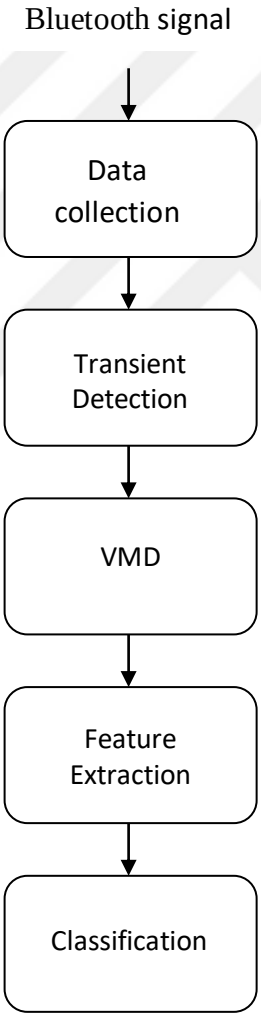

Figure 4.1 VMD based RF fingerprinting system

When the mobile device is switched on, the spreading signal of the device includes a channel noise portion, transient portion, and steady state portion. The transient part is produced by hard ware "manufacturing imperfection". The characteristics of this transient signal are generated from the instantaneous amplitude, instantaneous phase and instantaneous frequency. The VMD-RF fingerprinting system includes the following elements to be discussed:

1) Data collection: obtains the radio frequency signals generated by the emitting devices (Bluetooth devices).

2) Transient detection: is an important part in fingerprinting process, contains specific features of the emitting devices. Before transient detection, signal filtering is needed to reduce unwanted frequency components including noise.

3) Signal decomposition: In this subsystem VMD is applied to transient signals to create band-limited modes and to eliminate variations that may corrupt signals and affect signal identification.

4) Features extraction: The transient region of the being treated RF signals includes the particular characteristics of the emitting devices. These characteristics can be extracted at this stage.

5) Classification: This part of the system picks up the particular characteristics and establishes a relationship between the received RF signals and the transmission devices from which they were generated.

4.1. Data acquisition

The main purpose of our study is to test and examine the classification and identification steps correctly. This can be achieved using guaranteed real data and accurate procedures. Bluetooth signals were captured in the laboratory. The laboratory is located in an isolated location (underground) where no other equipment is operating, as any variation in temperature or humidity status may impact the accuracy of the identification. Temperature and humidity are kept constant in the laboratory. Figure 4.2 illustrates the signal collection system. The data is collected and stored in the laboratory.

The carrier frequency bandwidth of the Bluetooth signal ranges from 2400 MHz to 2483.5 MHz are received by a typical modem antenna and then delivered into an oscilloscope (4GHz).

In order to keep the (Signal/Noise) Ratio (SNR) at a high level, the distance between the antenna and the mobile phone is maintained about 30 cm.

The captured signals were digitized with ADC with a sampling frequency of at least 4.8 GHz. For a 2.4 GHz signal, the ADC should have a sampling frequency of at least 4.8 GHz, according to Nyquist theory.

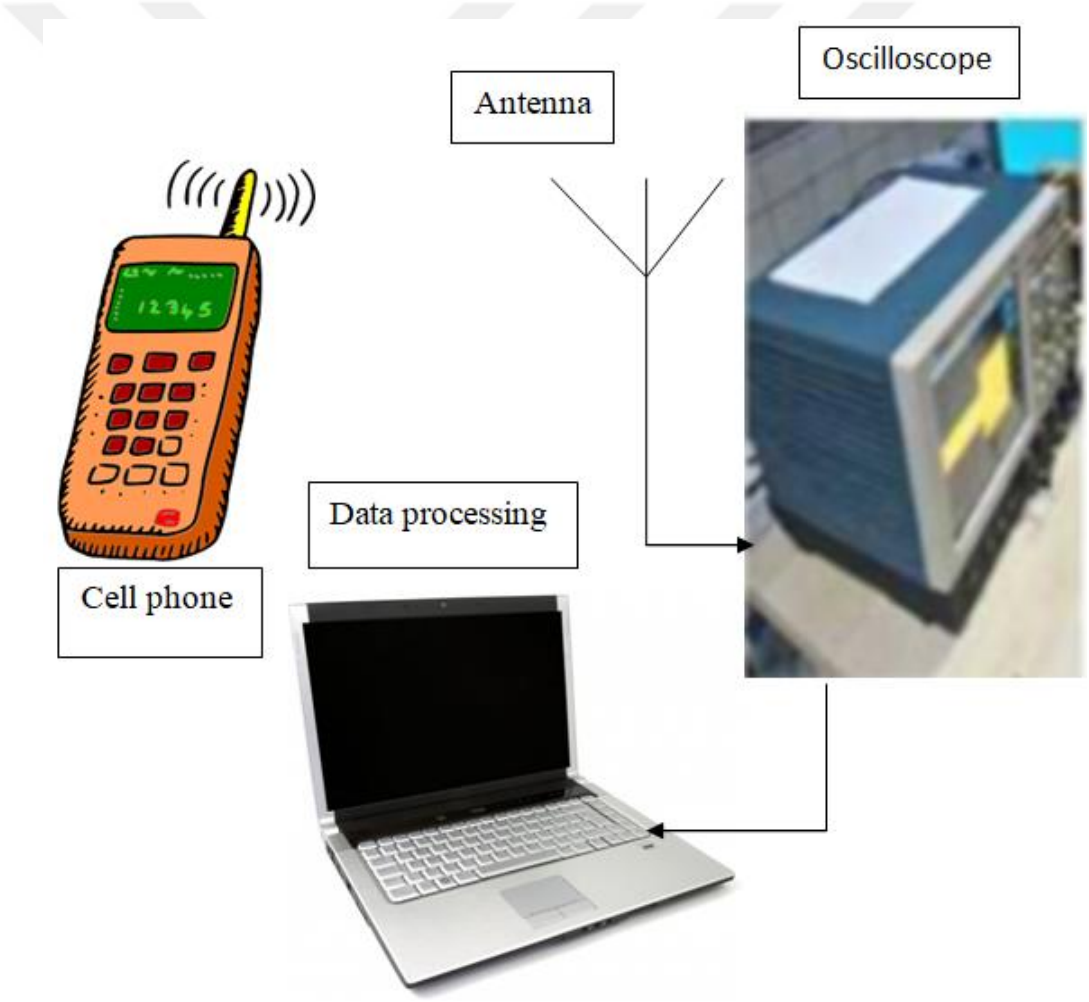

Figure 4.2 Signal acquisition systems

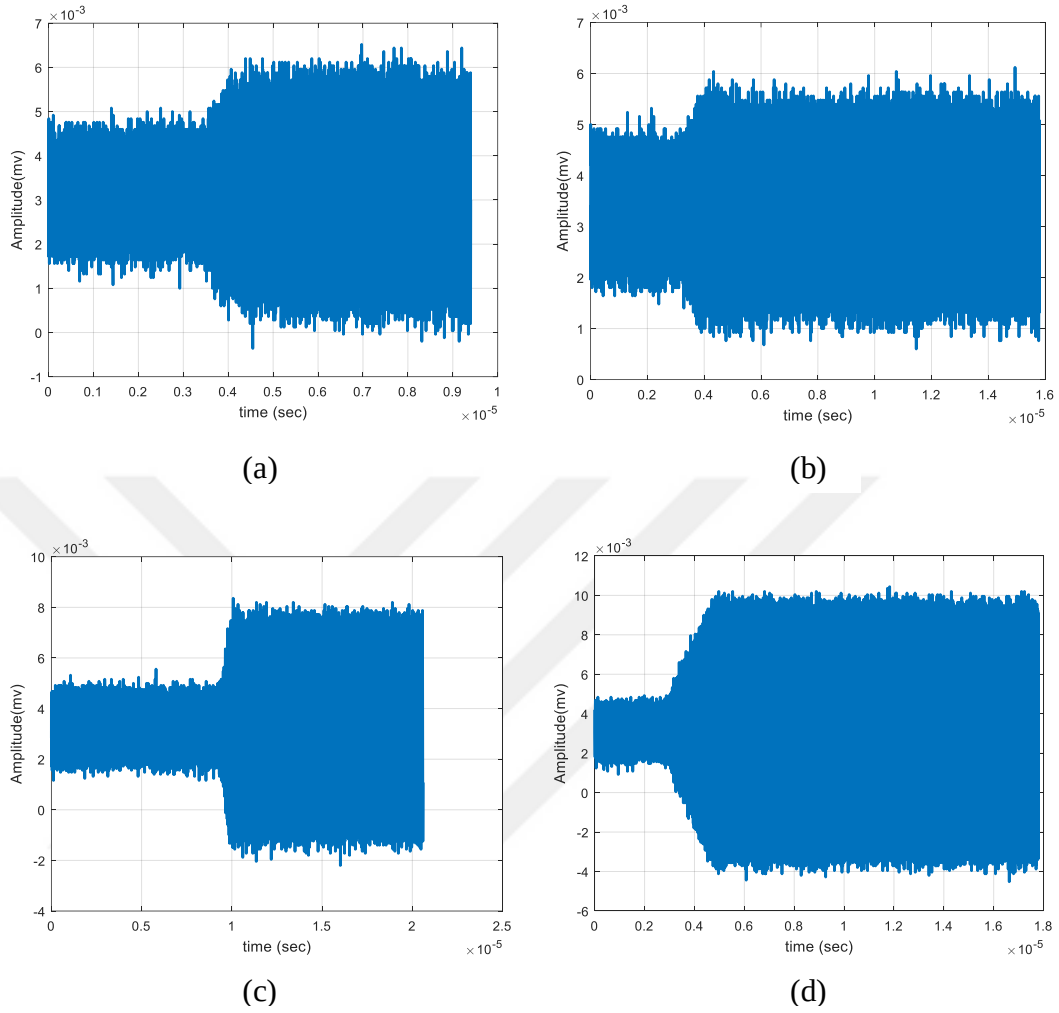

Figure 4.3 Collected BT signals. (a) Huawei-G5A,
(b) I-phone-7A , (c) LG-G4A, (d) Sony-C4A

Using this information, BT signals were recorded using a sampling frequency of 20 GHz. For example, typical forms of the four different signals collected are shown in Figure 4.3. These are collected from Huawei-G5A, Iphone-7A, LG-G4A and Sony-C4A respectively. Bluetooth signals radiated by mobile phones were received in the laboratory by an oscilloscope device of sampling rate (20 GSPS). One hundred and fifty Bluetooth signals were cached for each cell phone.

Five brands (Huawe, I-Phone, L-G, Samsung, and Sony) of ten various models were chosen for the testing. Two models were selected for each mobile phone brand, and two mobile phones with various serial numbers were selected for each model. Therefore, a data set of twenty mobile phones containing one hundred and fifty transient signals was formed for each mobile phone. These transient signals were sufficient to perform strong testing of identification success and extracted features. Mobile phones, models and brands are presented in Table 4.1. Characters A and B describe the serial number of devices of the same model and brand. Figure 4.4. shows the recorded signal which contains a noise portion , transient part and steady state part.

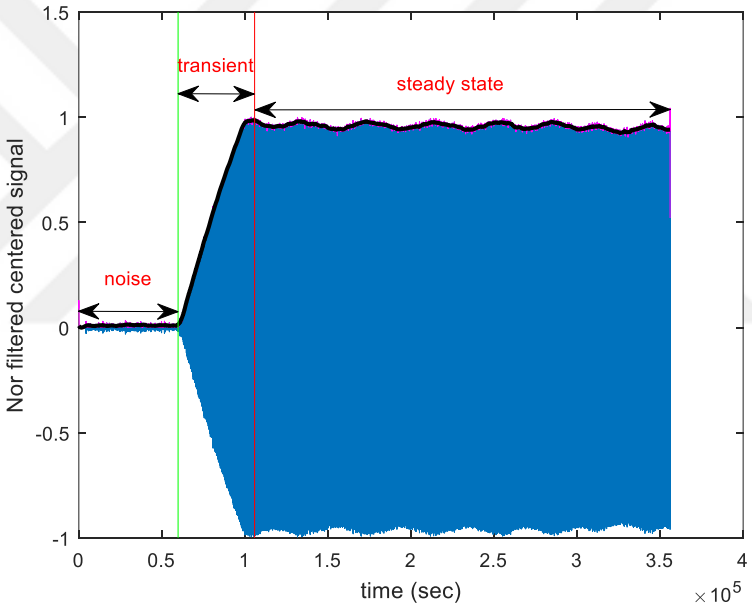

Figure 4.4 Filtered normalized BT signal

The recorded signals include unwanted frequency components produced after recording using an oscilloscope device, so filtering is required. The Band Pass Filter (BPF) is needed to remove these components. BPF with cut-off frequency 2400 MHz and 2485 MHz. Figure 4.5 illiterates the same signals as shown in Figure 4.3 But only after filtering and normalization. Since the transmitted signals have different amplitudes, normalization is needed to shift the amplitudes of the signals to the same level.

We need normalization because it scales all numeric variables between zero and one. In this case, normalization makes it easier to compare data from different locations.

Table 4.1. Brands and models of mobile phones

Class No.	Brand	Model
1	Huawe	G5 -A
2	Huawe	G5- B
3	IPhone	5S- A
4	IPhone	5S- B
5	IPhone	6S- A
6	IPhone	6S- B
7	IPhone	6S Plus -A
8	IPhone	6S Plus- B
9	IPhone	7 -A
10	IPhone	7 -B
11	L-G	G4 -A
12	L-G	G4- B
13	Sam-sung	Note3 -A
14	Sam-sung	Note3 -B
15	Sam-sung	S3- A
16	Sam-sung	S3 -B
17	Sam-sung	S4 -A
18	Sam-sung	S4 -B
19	Sony	C4- A
20	Sony	C4- B

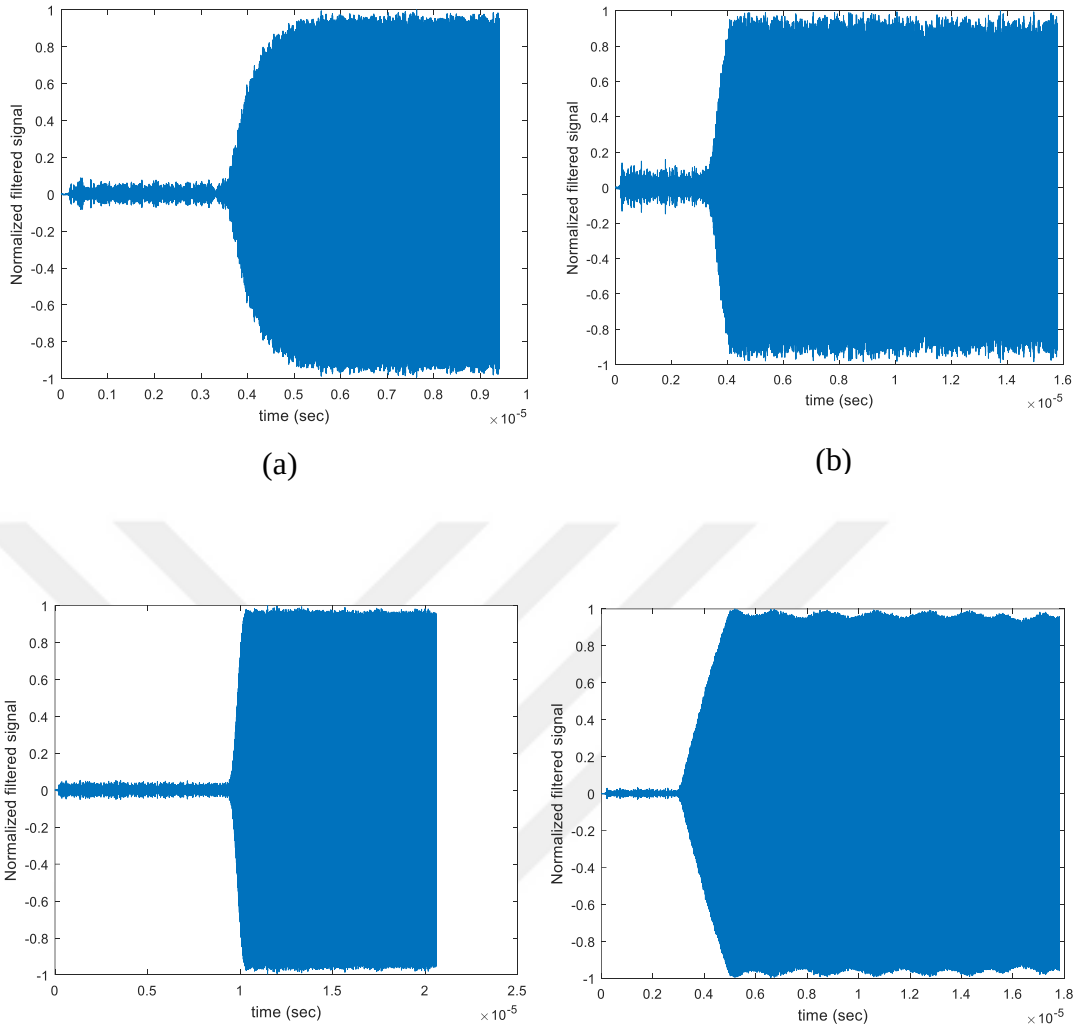

Figure 4.5 Filtered normalized transients of BT signals. (a) Huawei-G5A, (b) Iphone-7A, (c) LG-G4A, (d) Sony-C4A

4.2. Transient detection

Transient detection is required after the recorded signal is filtered. Transient detection is a very important step in the RF fingerprint process. If a transient signal is not detected precisely then the characteristics extracted from the received signal do not show the correct unique features of the transmitting devices.

Because in this case the detected transient signal will contain a part of the noise channel and a part of the steady state region. Detection process of transient signal is an important stage to classify and distinguish emitting devices with transient signal based RF fingerprinting approaches. Therefore the obtained transient signal should be filtered and normalized before the detection process. Transient detection can be obtained based on signal properties like (frequency, amplitude, energy and phase). In order to obtain accurate transient detection, implementation of different methods has been studied in the literature. These techniques depend on signal characteristics such as amplitude, phase and energy. The most popular transient detection method was based on the energy envelope of signal. This method was developed in [44] and was used for transient detection in our study. Fig 4.6 shows the detected transients of BT signals. The transient is detected from the transmitted signal via the following steps based on energy envelope [45]:

1. The signal should be filtered and normalized.
2. Obtaining the signal envelope by calculating the instantaneous amplitude of the transmitted signal using Hilbert Transform.
3. Window the energy envelope into non-overlapping windows.
4. Take the mean of the sliding windows, let the samples of the sliding windows start from i point.
5. Apply a threshold on the energy envelope and then compare the mean of the sliding window with the value of energy E(i) based on a certain threshold.
6. By the same technique the max local point at the end of the transient is detected.
7. The point is represented by the first positive slope of sliding window after the local maxima.

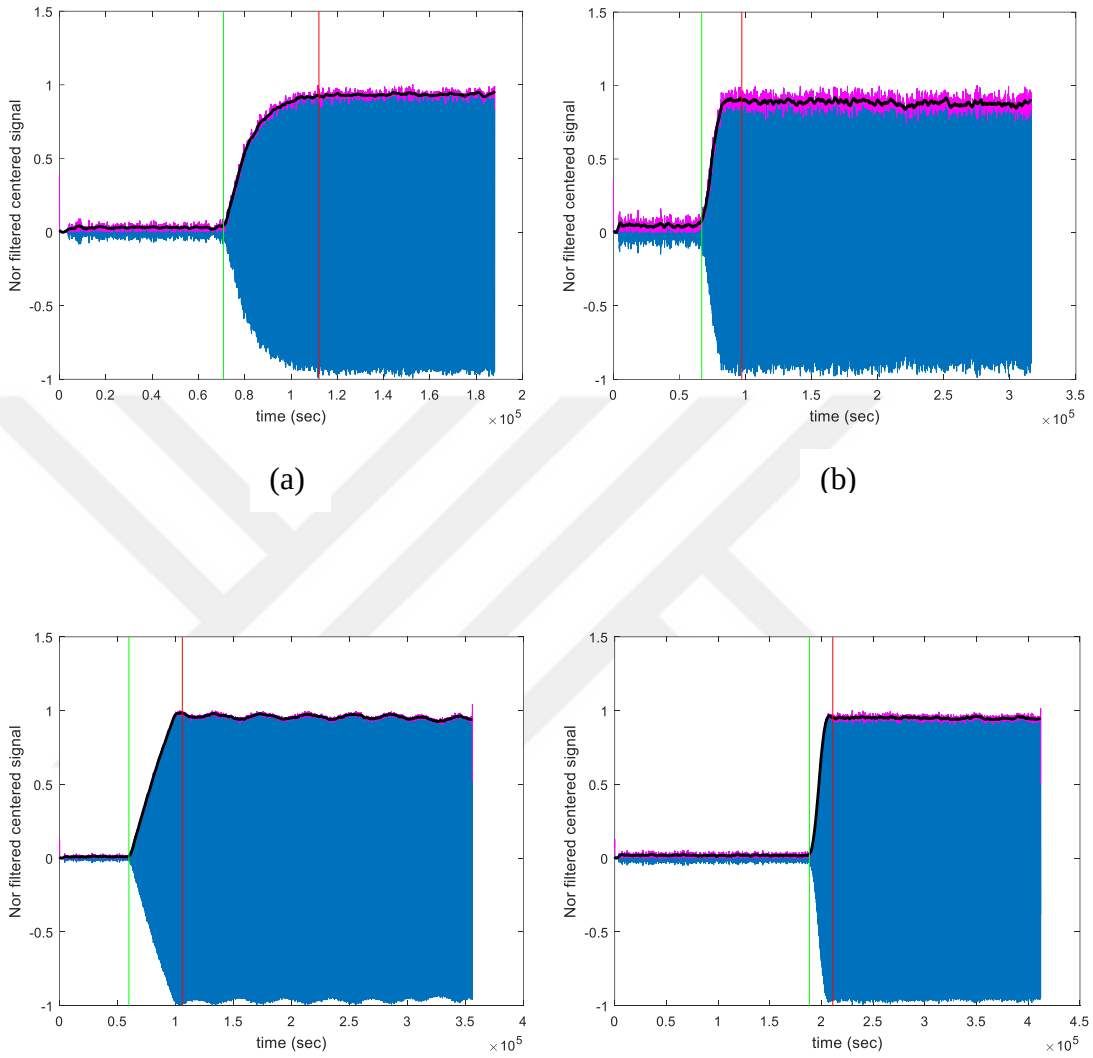

Figure 4.6 Detected transients of BT signals. (a) Huawei-G5A, (b) Iphone-7A, (c) LG-G4A, (d) Sony-C4A

To measure the success of the RF fingerprint approach with real noise situations, the recorded noise captured at various scales was randomly added to the captured transients that were originally received at a high level of (signal/noise) ratio (SNR). The SNR levels of the transient signals are decreased by adding portion of the recorded signal noise to the corresponding transient signals. The noise portion is weighted and added to the transient signal for each record of each class. The weight factors are varied such that the SNR levels of noisy transients are classified into different levels. For this objective, three variant data sets with various levels of SNR have been generated.

The SNR levels of the data sets are estimated at 1) low level (5 dB: 10 dB), 2) medium level (10 dB: 15 dB) and 3) high level (15 dB: 25 dB). They are the same datasets SNR levels used in the HHT method to compare the performance of both methods, VMD and HHT.

Three other datasets with lower SNR levels have been created to measure the performance of VMD-modes method compared with VMD-reconstruction transients' method. They estimated as (-5 : 0 dB), (0 : 5 dB) and (5 : 10 dB).

The SNR of the noisy transient are calculated based on the following equation:

$$SNR = 10 \log_{10} \left(\frac{s}{n} - 1 \right) \tag{4.1}$$

Where *(s)* is noisy signal and (*n*) is noise.

The symmetric distribution of the noisy transient SNR levels is generated to match the Gaussian distribution (see the histogram in Fig 4.7 and Fig 4.8), so that the median of noisy transients SNR approximately equal its mean. This guarantees an appropriate distribution of the data SNR of all SNR levels. Consequently, sensible results can be achieved. Once the different levels of noisy transient are generated the overall features are extracted from the noisy transients.

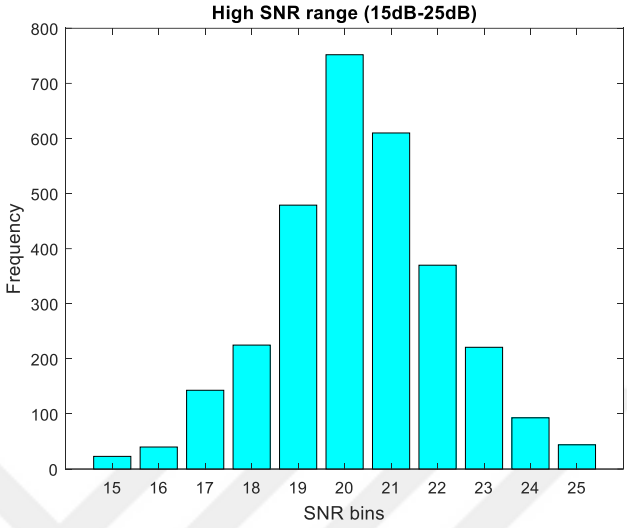

Figure 4.7 A histogram of SNR values of noisy transient records (15dB-25dB)

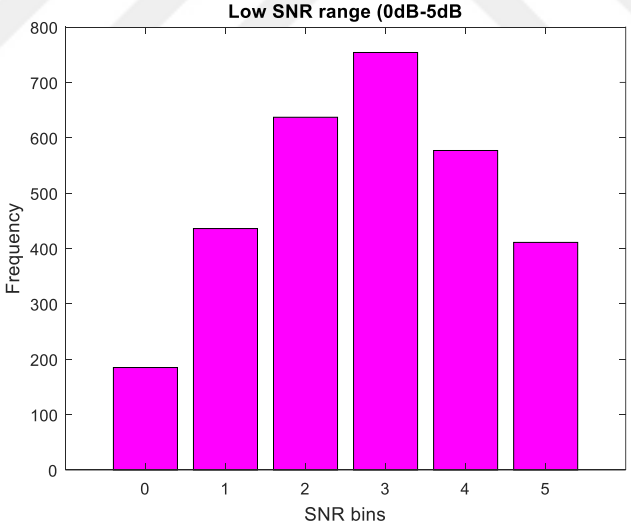

Figure 4.8 A histogram of SNR values of noisy transient records (0dB-5dB)

4.3. Features extraction

The BT transmitted signal contains a RF fingerprint. The signal RF fingerprint is associated with the cell phone brand, model and serial number. The RF fingerprint composed of bunch of unique features. The characteristics of signal such as instantaneous frequency $f(n)$, instantaneous amplitude $a(n)$ and phase $\emptyset(n)$ can be used to obtain the RF fingerprint.

To compute $a(n)$, $\emptyset(n)$ and $f(n)$, the real transient signal x(n) is transformed into analytic signal (I and Q data) by a Hilbert transform [46]. The complex form is useful in the calculating of instantaneous amplitude, frequency and phase. We can define the complex signal $\hat{x}(n)$ as

$$\hat{x}(n) = x(n) + jH\{x(n)\} = A(n)e^{j\theta(n)} \tag{4.2}$$

$$\hat{x}(n) = x(n) + j(h(n) * x(n)) \tag{4.3}$$

Where the impulse response h(n) = $\frac{1}{\pi n}$.

The complex time domain signal $\hat{x}(n)$ written in the expression:

$$\hat{x}(n) = \hat{x}_I(n) + \hat{x}_Q(n) \tag{4.4}$$

Instantaneous amplitude, $a(n)$, phase, $\emptyset(n)$, and frequency, $f(n)$, given by

$$a(n) = \sqrt{[\hat{x}_I(n)]^2 + [\,\hat{x}_Q(n)\,]^2} \tag{4.5}$$

$$\emptyset(n) = tan^{-1}\left[\frac{\hat{x}_Q(n)}{\hat{x}_I(n)}\right], \tag{4.6}$$

$$f(n) = \frac{\emptyset(n) - \emptyset(n-1)}{2\pi\Delta(n)} \tag{4.7}$$

The instantaneous amplitude, frequency response and phase are simply centered using

$$a_c(n) = a(n) - \mu_a \tag{4.8}$$

$$f_c(n) = f(n) - \mu_f \tag{4.9}$$

$$\emptyset_{cnl}(n) = \emptyset_{nl}(n) - \mu_{\emptyset nl} \tag{4.10}$$

Where N is the number of samples in the signal and μ_a , μ_f are amplitude and frequency means. $\emptyset_{nl}(n)$ is the resultant non-linear phase response given by

$$\emptyset_{nl}(n) = \emptyset(n) - 2\pi\mu_f(n)\Delta t \tag{4.11}$$

Then the sequences $a_c(n)$, $f_c(n)$ and $\emptyset_{cnl}(n)$ are normalized by dividing by the maximum value. Statistics are calculated after the sequences are centered and normalized [47-50]. The statistics for a randomly centered and normalized sequence $v(k)$ with N_v samples are:

$$\sigma_v^2 = \frac{1}{N_v}\sum_{k=1}^{N_v}[v(k) - \bar{v}]^2 \tag{4.12}$$

$$\gamma_v = \frac{1}{\sigma_v^3 N_v}\sum_{k=1}^{N_v}[v(k) - \bar{v}]^3 \tag{4.13}$$

$$k_v = \frac{1}{\sigma_v^4 N_v}\sum_{k=1}^{N_v}[v(k) - \bar{v}]^4 \tag{4.14}$$

Where $v(k)$ represents any of the sequences given in equations (4.12), (4.13), and (4.14) after they normalized. The number of features can be created by using these sequences with these three high order statistics. The purpose of RF fingerprinting process is to get sufficient properties to classify the BT transceiver from other transceivers.

The features that are used in this study are created from the reconstructed transient signals and the decomposed modes of the transient signals. Nine features are generated from each reconstructed transient signal and twenty seven features from decomposed modes (nine features of each mode). The main features are illustrated in Table 4.2. To show the robustness of created features before applying the classifier, two types of plots are used, namely, box plot and conventional two dimensional Matlab plot. Characteristics of the descriptive statistics can be visualized by means of boxplot of data. The boxplot (see Fig.4.9) is a standard way of showing data distribution based on a five criteria:

The minimum, first quarter Q1, second quartile Q2, third quartile Q3 and the maximum. The first quartile (1st quarter) is the value of the data tested, with twenty-five percent of the data values less than (Q1) point. The second quartile (2nd quarter) also called the median is the value that located between the first and the third quartiles, which equal fifty percent of the data set or the interquartile range (IQR). The interquartile is defined as the length of data box (IQR=Q3-Q1). Twenty-five percent of data values are greater than the third quartile (Q3) point. The red line in the middle of data box clarifies the fifty percent of data values. The whisker limits are indicated by the minimum (lower adjacent) value and the maximum (upper adjacent) value.

These limits can be calculated by multiplying the interquartile range (IQR) by the value (1.5) and add to the seventy- five percent (Q3) to get the maximum limit or subtract from the twenty- five percent (Q1) to get the minimum limit. Outlier values are data set values outside the whisker limits [51].

The widely used box plot is implemented to the variance (VAR) of transient signals' instantaneous phases of the twenty introduced classes. That is illustrated in Fig. 4.10 and Fig. 4.12. By means of the box plot a clear picture of the interference among classes feature can be seen. Moreover, by using the box plot, the percentage of the data concentration can be recognized. As seen from Fig.4.10, there are statistically significant differences between some of the statistics of different classes while some of them are close to overlap. If the box values included the whiskers for a given device are separated from the box values of the other devices considered, the feature can be fully separated and if only the whiskers are not separated, then the device being considered will be almost separable feature.

Because of the separation property, the variance (VAR) of transient signal instantaneous phase is one of the most robust features. This feature is created from instantaneous characteristics of the reconstructed transient signal. VAR of reconstructed transient signals' instantaneous phases of the twenty introduced classes with 150 records is introduced as an example of the robust features. Fig. 4.11 and Fig 4.13 show a conventional two dimensional Matlab plot of the (VAR) of reconstructed transient signals' instantaneous phases. It's appered from Fig. 4.11 that some classes are completely separated. For instant, class_20 (Sony C4 B) is completely separated from class_1 through class_18, however class_20 is partially separated (nearly separable) from class_19 (Sony C4 A). Some other classes are nearly separable such as class_1 (Huawei G5 A) and class_2 (Huawei G5 B). However, there are some classes are barely separated such as class_15 (SamSung_S3_A) and class_16 (SamSung_S3_B). The advantage of the conventional two dimensional Matlab plot is that by which we can know the number of interfered records and interfered records' numbers for each class.

Table 4.2 Features list

Feature lable	Feature name
F1	Variance of transient instantaneous phase
F2	Kurtosis of transient instantaneous phase
F3	Skewness of transient instantaneous phase
F4	Variance of transient instantaneous amplitude
F5	Kurtosis of transient instantaneous amplitude
F6	Skewness of transient instantaneous amplitude
F7	Variance of transient instantaneous frequency
F8	Kurtosis of transient instantaneous frequency
F9	Skewness of transient instantaneous frequency

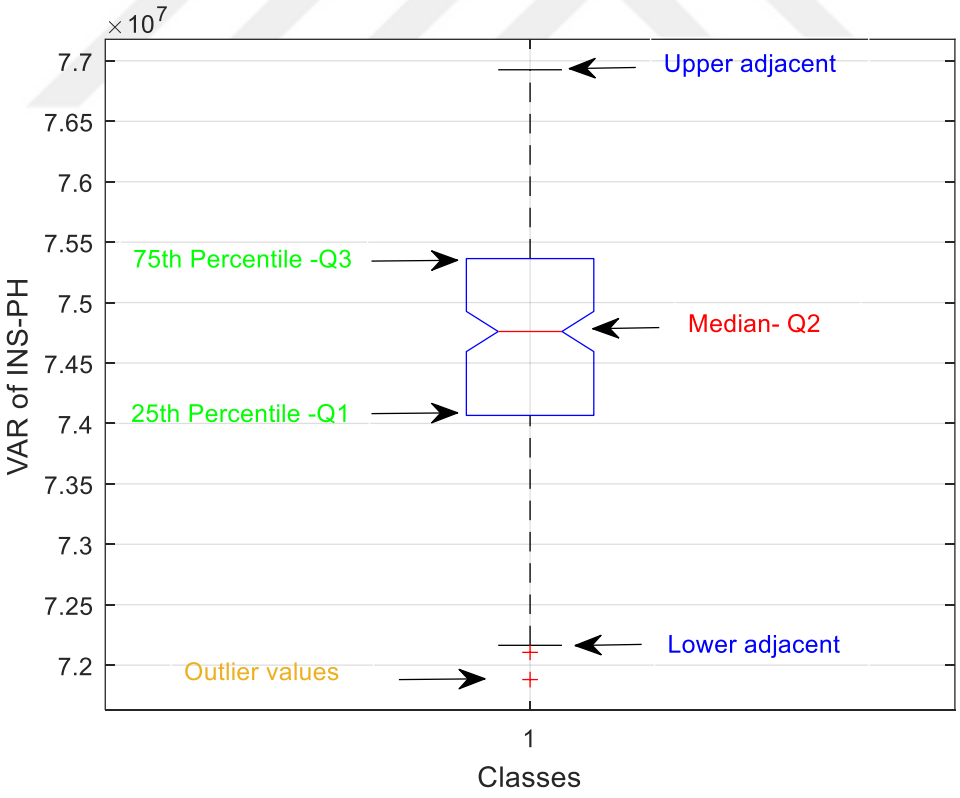

Figure 4.9 Box plot criteria

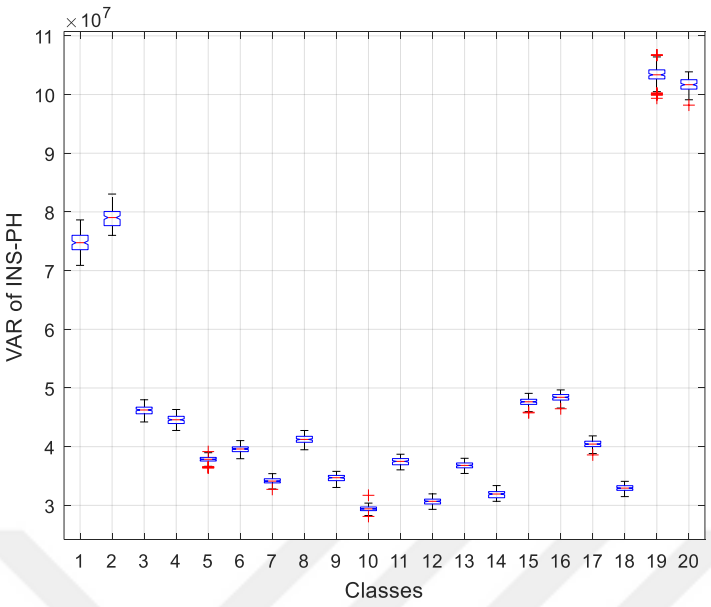

Figure 4.10 Box plot of VAR of trans. ins. phases(15 dB-25 dB)

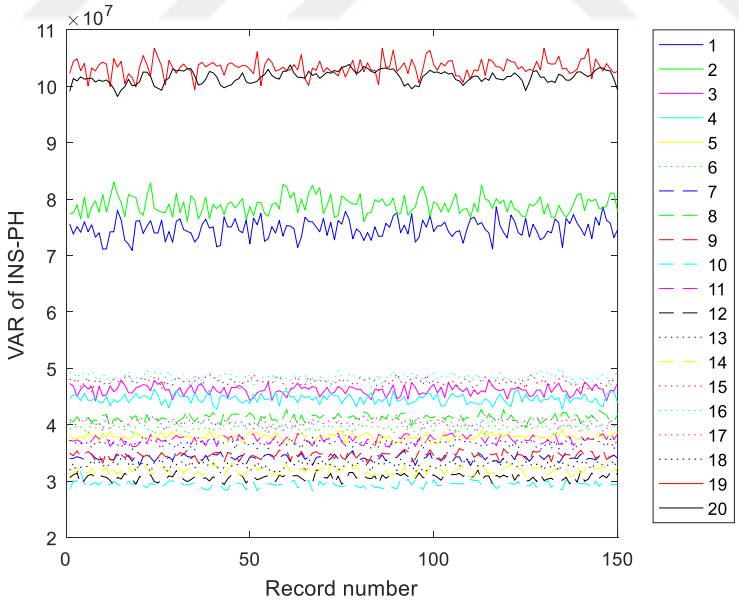

Figure 4.11 Conventional plot of VAR of trans. ins. phases(15 dB-25 dB)

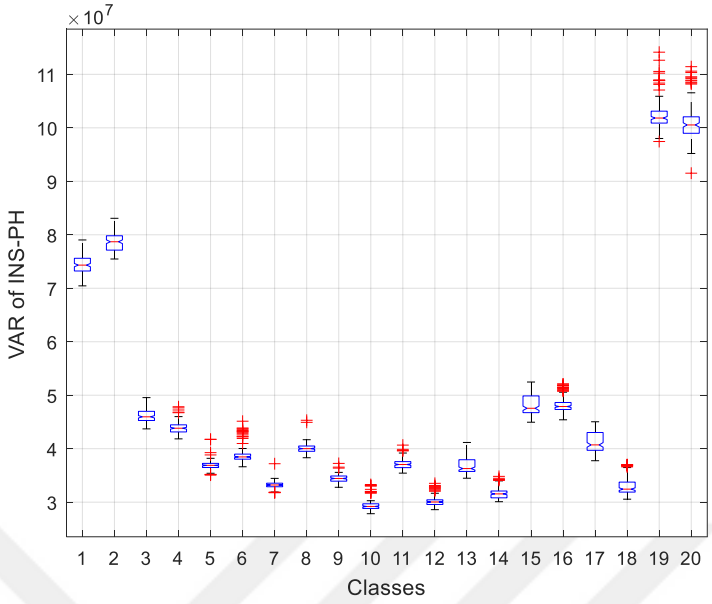

Figure 4.12 Box plot of VAR of trans. ins. phases(5 dB-10 dB)

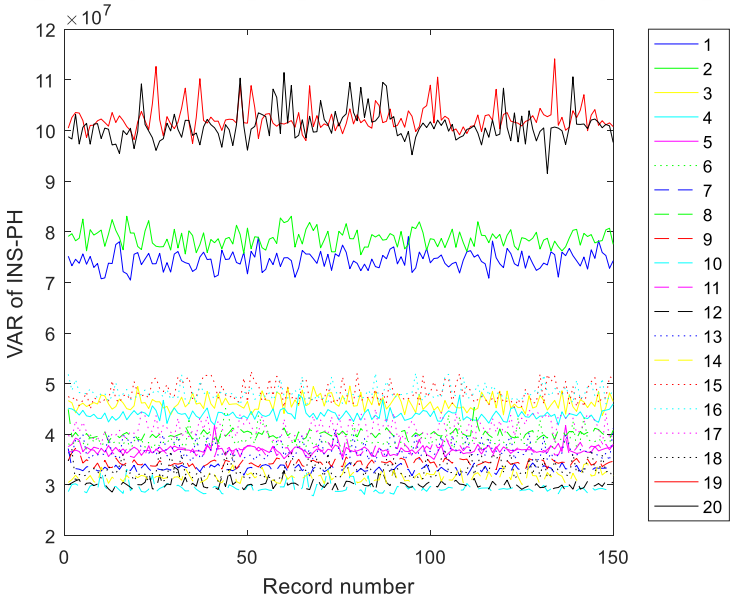

Figure 4.13 Conventional plot of VAR of trans. ins. phases(5 dB-10 dB)

4.4. Classification

When a series of characteristic vectors are created, classification can be made. To be able to classify, characteristic vectors must be divided by training data and testing data for each Bluetooth device. Training process presented to establish a relationship between characteristic vectors and the BT device in which they are formed. The process is accomplished by providing the classifier with a characteristic vector and a corresponding BT device tag for all characteristic vectors in the training set. Next, a test set of characteristic vectors is applied to predict the success of the classifier. At this step, the classifier is fed with each unlabeled characteristic vector in the testing data, and the classifier bring back the tag of the BT device that most correspond to the characteristic vectors.

In this work, the nine characteristics that have been created used to perform the RF fingerprinting of 20 devices each containing 150 records (transients). The created characteristics are segmented into training data and test data, so that each feature created by each device is segmented into the training data group by forty percent and the test data group by sixty percent of the overall data. For each set of data, a linear support vector machine (LSVM) is applied.

LSVM is an intelligence technique depended on theoretical basis of powerful statistical learning that is effectively implemented in many real data tests, like pattern estimation and devices identification [7]. LSVM applied in two stages for identification objective. In the 1st stage, LSVM is trained with the data group that is selected as training set. As soon as the LSVM is trained, the decision equation of LSVM is estimated:

$$f(x) = sign(\omega . \emptyset(x) + b), \tag{4.15}$$

In the 2nd stage, an LSVM is applied to the test data for classification according to the decision equation specified in the training stage.

. The classification function is defined as:

$$f(x) = sign\left[\left(\sum_{i=1}^{L} \propto_i y_i K(x_i, x_j)\right) + b\right] \tag{4.16}$$

Where $K(x_i, x_j)$ is kernel function, $\propto_i$ is i-th mode embedded dimension. Further description of LSVM in [52–54]. RF fingerprint of extracted features is representing the subjected data for classifiers. The classifier is firstly trained and then applied to the test data.

The training stage of each classification process generates model. The generated model is used to classify the classes based on the test data. In this study we considered the classification accuracy of VMD in two cases. The first case, we measure the classification performance of VMD method using nine features of the reconstructed transients under deferent SNR levels, 5 dB: 10 dB, 10 dB : 15 dB and 15 dB : 25 dB then compared with an existing method (HHT). In the second case, we determine the classification performance of VMD using twenty seven features of VMD-modes under deferent SNR levels, -5 dB : 0 dB, 0 dB : 5 dB and 5 dB : 10 dB then compared with the classification performance of VMD-reconstructed transients.

4.4.1 Classification performance of VMD against HHT method

The LSVM classifier is applied to train data to generate a classifier model. The generated model is utilized to classify the test data based on the classifier training or learning. The training confusion matrices based on 40% train of high SNR range (15 dB-25 dB) and low SNR range (5 dB-10 dB) datasets are illustrated in Fig. 4.14 and Fig. 4.16, respectively.

The training confusion matrices demonstrate 97.8% and 96.8% for high SNR range and low SNR range respectively. The features F1 (VAR of ins. phase) against F6 (SKEW of ins. amplitude) of transient are plotted as scatter plot of the train data for 20 classes (see Fig. 4.15). The scatter plot of the same features for low SNR range is shown Fig. 4.17. It's deduced from the features scatter plots that the features' plots of each class records are close to each other for high SNR range compared with low SNR.

The LSVM classifier is used to test a set of data representing 60% of the overall data to estimate the performance of the classifier after the training procedure. Linear support vector machine (LSVM) is the most popular technique. It has been tested and compared with other data classification techniques and achieved the highest performance for Bluetooth signals [45].

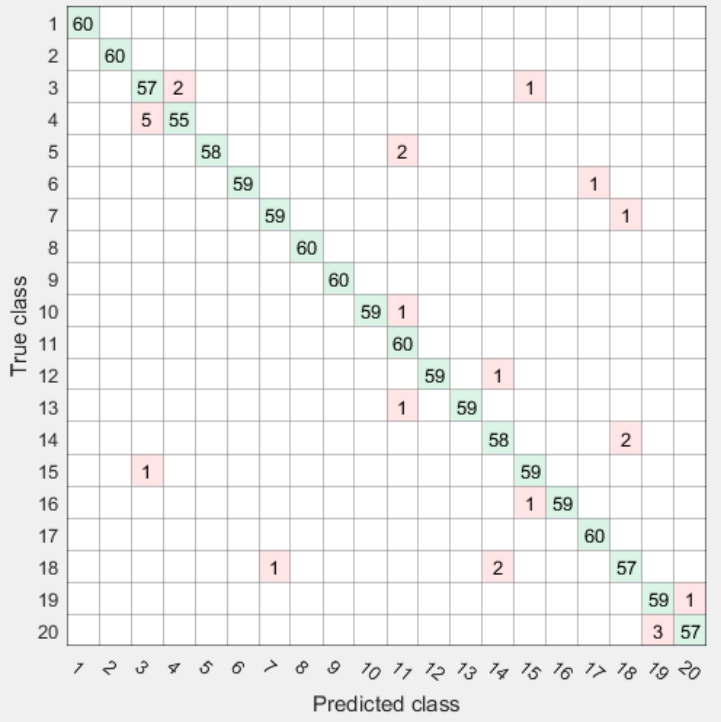

Figure 4.14 Confusion matrix based on 40% of train data (15dB-25dB)

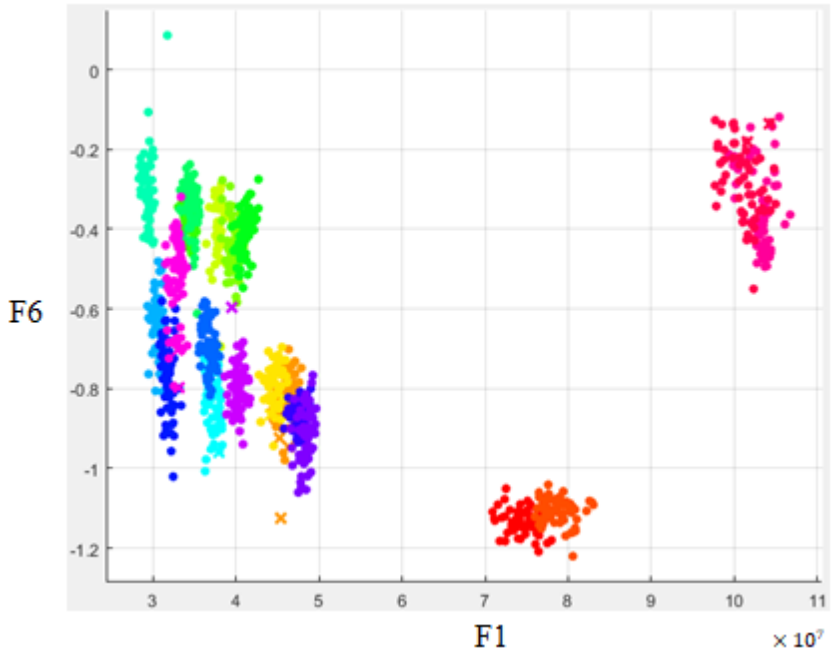

Figure 4.15 Scatter plot of data features F1 vs. F6 (15dB-25dB)

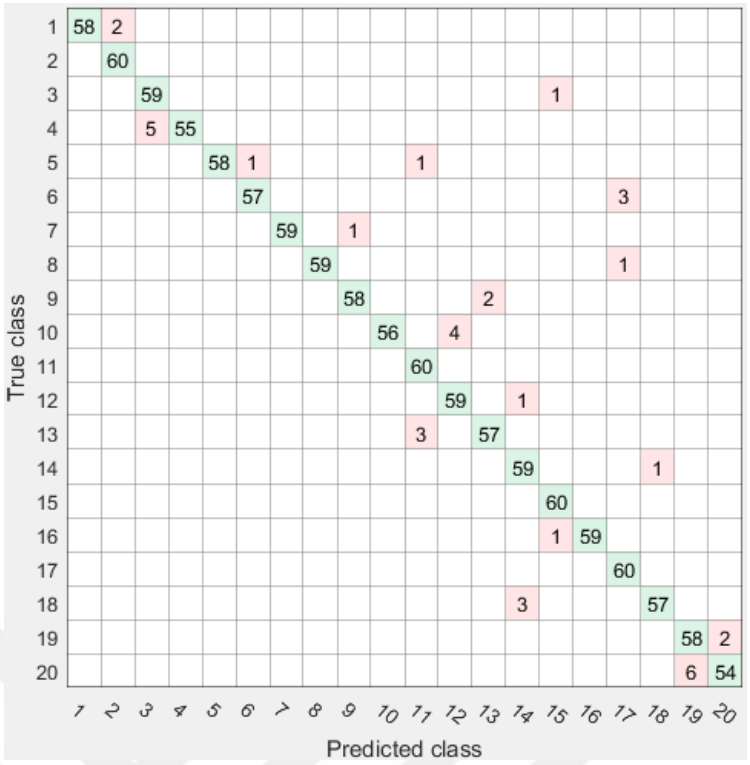

Figure 4.16 Confusion matrix based on 40% of train data (5dB-10dB)

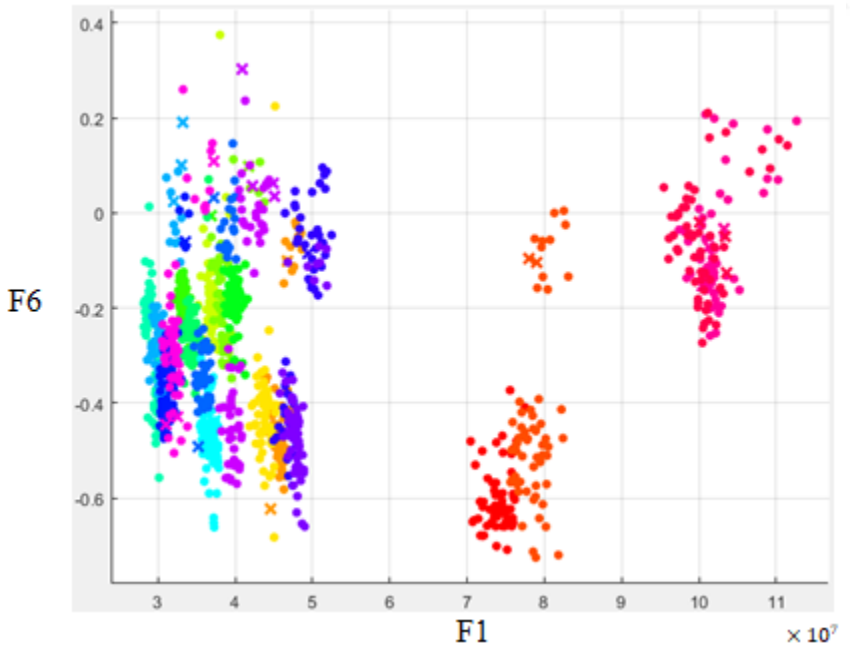

Figure 4.17 Scatter plot of data features F1 vs. F6 (5dB-10dB)

Therefore, in our study, LSVM was selected for BT dataset classification. Fig. 4.18 through Fig. 4.20 show the confusion matrices for twenty Bluetooth transceivers (cell phones) with low SNR level moderate SNR and high SNR, when the classification results based on VMD reconstructed transients. Fig. 4.18 illustrates the confusion matrix for twenty Bluetooth transceivers (cell phones) with low SNR level (5dB-10dB). The first column shows the actual class and the remaining columns show the predicted class. For example, when class 9 (I-Phone 7A) is tested for classification in low SNR, it is identified 84.4% correctly as class 9 and 15.6 %, is miss-classified as class 7 (I-Phone 6S).

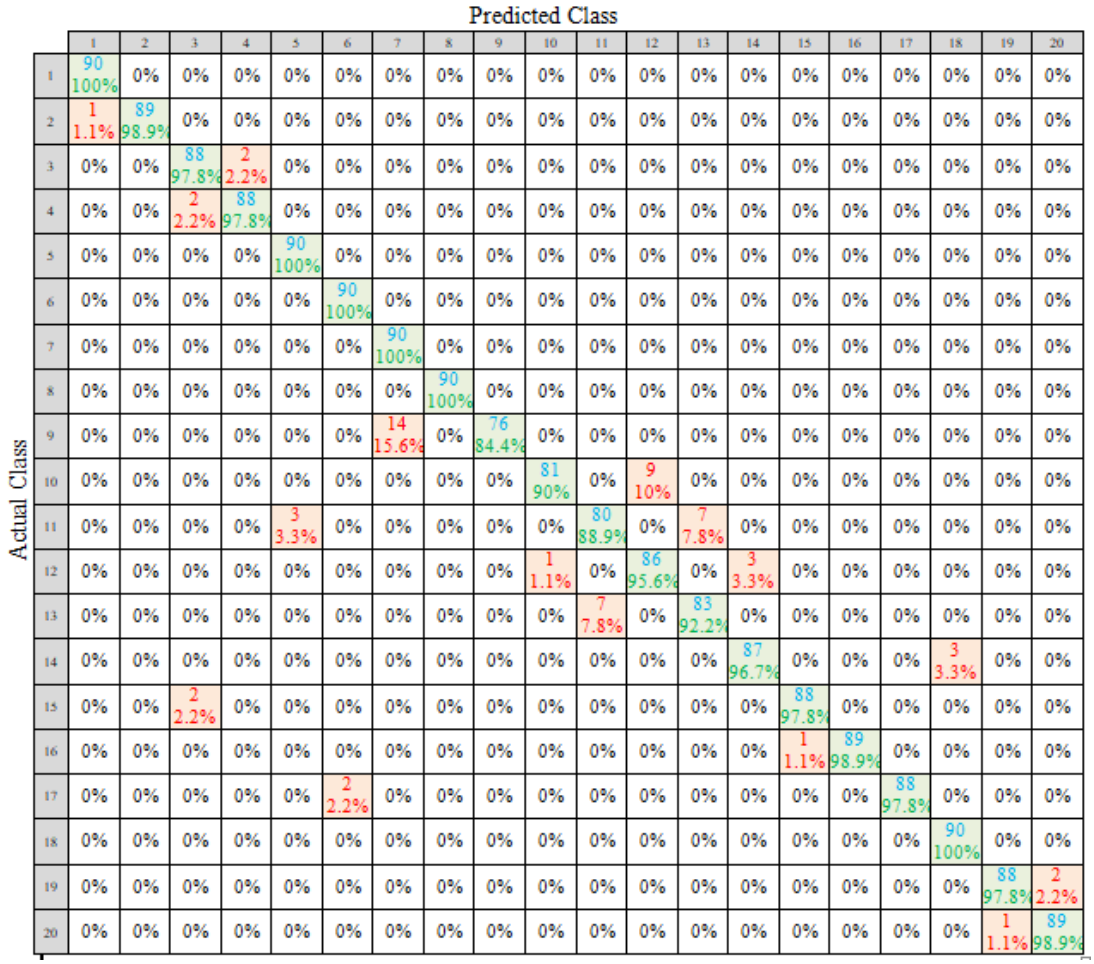

Figure 4.18 Confusion matrix at low SNR range (5dB-10dB)

However by comparing the classification in moderate SNR and high SNR, class 9 is identified 94.4 % and 95.6% respectively. While 5.6 % and 4.4% are miss-classified as class 7 in moderate SNR and high SNR, respectively. The testing shows different performances for three different SNR ranges of the input data as presented in Table 4.3. It concluded that the correct classification rate of low SNR, moderate SNR and high SNR is 96.7%, 98.0% and 98.4%. While 59, 36 and 28 records (transients) are miss-classified out of one thousand eight hundred transient as test data in the confusion matrix for low level (SNR), moderate level (SNR) and high level (SNR), respectively.

Predicted Class

Actual Class	1	2	3	4	5	6	7	8	9	10	11	12	13	14	15	16	17	18	19	20
1	88 97.8%	2 2.2%	0%	0%	0%	0%	0%	0%	0%	0%	0%	0%	0%	0%	0%	0%	0%	0%	0%	0%
2	0%	90 100%	0%	0%	0%	0%	0%	0%	0%	0%	0%	0%	0%	0%	0%	0%	0%	0%	0%	0%
3	0%	0%	89 98.9%	0%	0%	0%	0%	0%	0%	0%	0%	0%	0%	0%	1 1.1%	0%	0%	0%	0%	0%
4	0%	0%	0%	90 100%	0%	0%	0%	0%	0%	0%	0%	0%	0%	0%	0%	0%	0%	0%	0%	0%
5	0%	0%	0%	0%	90 100%	0%	0%	0%	0%	0%	0%	0%	0%	0%	0%	0%	0%	0%	0%	0%
6	0%	0%	0%	0%	2 2.2%	87 96.7%	0%	0%	0%	0%	0%	0%	0%	0%	0%	0%	1 1.1%	0%	0%	0%
7	0%	0%	0%	0%	0%	0%	90 100%	0%	0%	0%	0%	0%	0%	0%	0%	0%	0%	0%	0%	0%
8	0%	0%	0%	0%	0%	0%	0%	90 100%	0%	0%	0%	0%	0%	0%	0%	0%	0%	0%	0%	0%
9	0%	0%	0%	0%	0%	0%	5 5.6%	0%	85 94.4%	0%	0%	0%	0%	0%	0%	0%	0%	0%	0%	0%
10	0%	0%	0%	0%	0%	0%	0%	0%	0%	83 92.2%	0%	7 7.8%	0%	0%	0%	0%	0%	0%	0%	0%
11	0%	0%	0%	0%	0%	0%	0%	0%	0%	0%	90 100%	0%	0%	0%	0%	0%	0%	0%	0%	0%
12	0%	0%	0%	0%	0%	0%	0%	0%	0%	0%	0%	89 98.9%	0%	1 1.1%	0%	0%	0%	0%	0%	0%
13	0%	0%	0%	0%	0%	0%	0%	0%	0%	0%	3 3.3%	0%	87 96.7%	0%	0%	0%	0%	0%	0%	0%
14	0%	0%	0%	0%	0%	0%	0%	0%	0%	0%	0%	0%	0%	90 100%	0%	0%	0%	0%	0%	0%
15	0%	0%	3 3.3%	0%	0%	0%	0%	0%	0%	0%	0%	0%	0%	0%	87 96.7%	0%	0%	0%	0%	0%
16	0%	0%	0%	0%	0%	0%	0%	0%	0%	0%	0%	0%	0%	0%	1 1.1%	89 98.9%	0%	0%	0%	0%
17	0%	0%	0%	0%	0%	1 1.1%	0%	1 1.1%	0%	0%	0%	0%	0%	0%	0%	0%	88 97.8%	0%	0%	0%
18	0%	0%	0%	0%	0%	0%	0%	0%	0%	0%	0%	0%	0%	2 2.2%	0%	0%	0%	88 97.8%	0%	0%
19	0%	0%	0%	0%	0%	0%	0%	0%	0%	0%	0%	0%	0%	0%	0%	0%	0%	0%	85 94.4%	5 5.6%
20	0%	0%	0%	0%	0%	0%	0%	0%	0%	0%	0%	0%	0%	0%	0%	0%	0%	0%	1 1.1%	89 98.9%

Figure 4.19 Confusion matrix at moderate SNR range (10dB-15dB)

By comparing the classification performance of VMD method and the Hilbert-Huang Transform (HHT) approach, we concluded that the VMD method was much better than the HHT approach [45]. We also note that class 9 (IPhone 7-A) offers the highest transient misclassified cases. A general comparison of the identification accuracy of VMD and HHT methods is recorded in Table 4.3. Even though the number of features in our study is lower than the number of features in the HHT approach [45], the classification accuracy of VMD is still better.

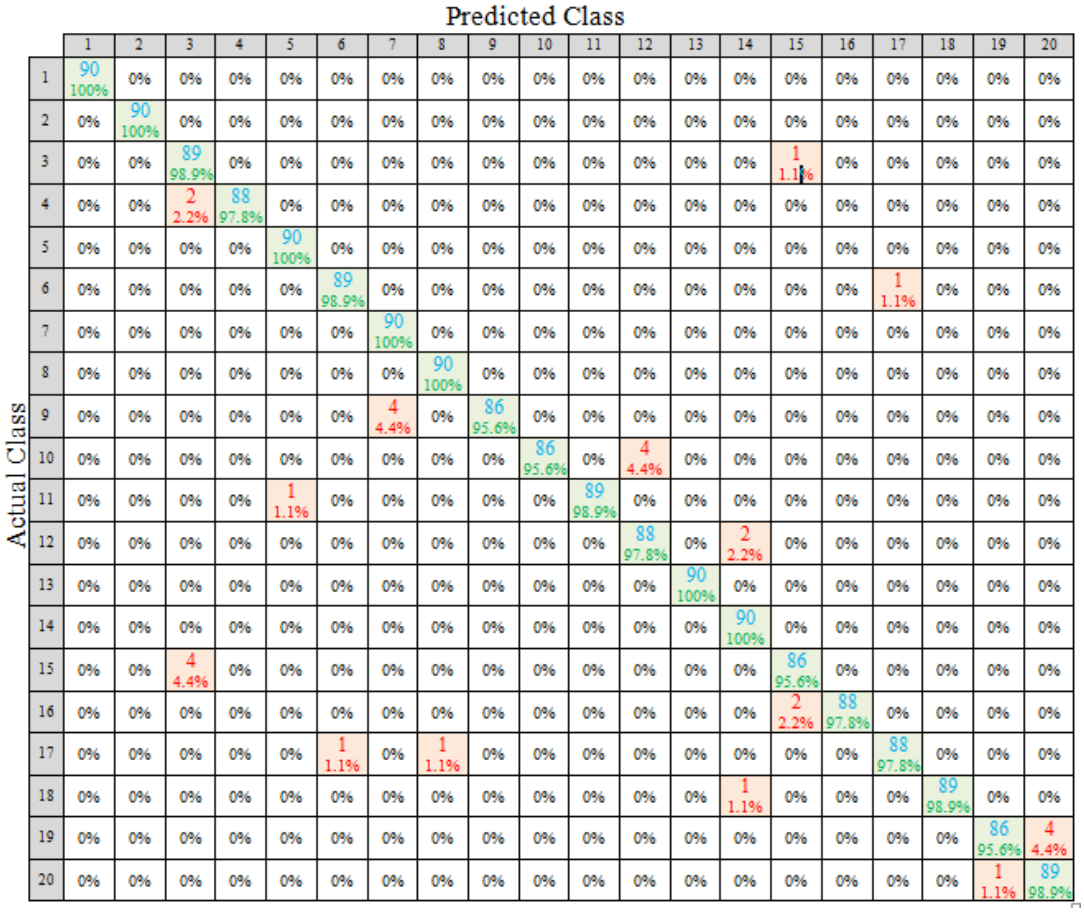

Figure 4.20 Confusion matrix at high SNR range (15dB-25dB)

Furthermore, we noted that the SNR values used in the VMD method are (2-3 dB) lower than the SNR values in [45]. Moreover, when the performance of the HHT method in classifying the classes was examined, it was found that many I-Phone classes (Fig.13 of [45]) were mis-classified at low SNR levels with a correct classification rate of 35% and 44.4%.

While in the VMD method the correct classification rates were 84.4% and 100% respectively. In the VMD-reconstructed transients method, the highest misclassified rate was for I-Phone 7 A, where 15.6% of the transients mis-classified as I-Phone 6S-Plus and the correct classification rate was 84.4%.

Table 4.3 Performance results of VMD and HHT [45]

Method/SNR Level	Low	Moderate	High
Proposed method (VMD)	96.7% (5:10 dB)	98.0% (10:15 dB)	98.4% (15:25 dB)
Hilbert-Huang Transform (HHT) [45]	79.3% (8:10 dB)	82.1% (12:15 dB)	90.5% (18:23 dB)

4.4.2 Classification performance of VMD-modes

Twenty BT devices each with 150 transients of different models and serial numbers which presented in table 4.1 are used in this study. Nine features perform the RF fingerprints of Bluetooth classess are extracted of each reconstructed transient. Fig. 4.21 shows the amplitude skewness and phase variance of VMD-reconstructed transients. Twenty seven feature vectors are extracted for the three decomposed modes (Nine features each mode).

Fig. 4.22 shows the amplitude skewness and phase variance of VMD-modes. As seen from these figures, there are statistically significant differences between some of the statistics of different classes while some of them are close to overlap. LSVM classifier was trained with a 40% training data (sixty records per class) of the overall data (one hundred and fifty records per class).

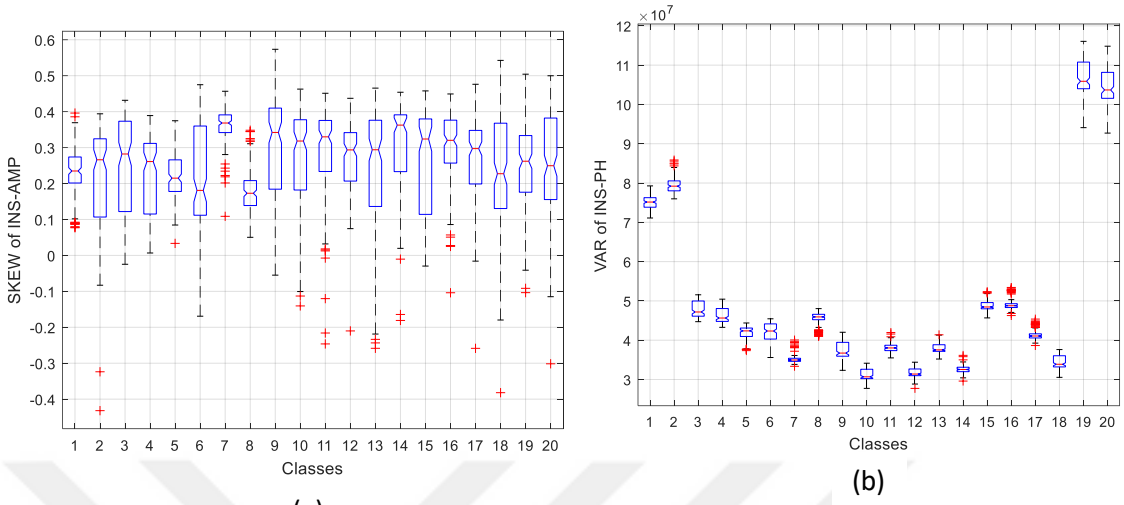

Figure 4.21 Features of VMD-reconstructed transients for 20 cell phones. (a) SKEW of INS-AMP, (b) VAR of INS-PH

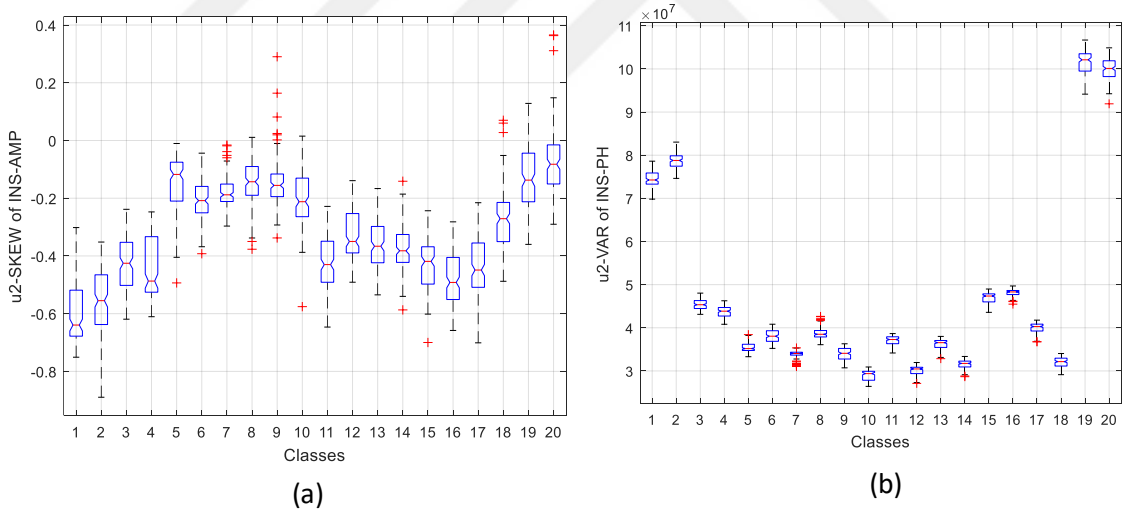

Figure 4.22 Features of VMD-modes for 20 cell phones. (a) SKEW of INS-AMP for mode2, (b) VAR of INS-PH for mode2

After the LSVM training, it is supplied with test data containing 60% (ninety records per class) of the overall data set. Fig. 4.23 through Fig. 4.26 show the confusion matrices for twenty Bluetooth devices under low SNR (-5 dB : 0 dB) and moderate SNR level (0 dB : 5 dB) for VMD- reconstructed transient method and VMD- modes method.

The first column of each confusion matrix represents the output class, the remaining columns show the target class and the diagonal represents the percentage of correct classification. Testing shows different performances under three different SNR ranges of the input data is recorded in Table 4.4.

As presented in the table the correct classification average of low SNR level, moderate SNR level and high SNR level is 67.5%, 87.3% and 96.7% based on VMD-reconstructed transients and 70.1%, 91.0% and 97.1% based on VMD-decomposed modes.

Table 4.4 Classification accuracy

Method/SNR Level	Low (-5 : 0 dB)	Moderate (0 : 5 dB)	High (5 : 10 dB)
VMD-modes method	70.1%	91.0%	97.1%
VMD-reconstructed transient method	67.5%	87.3%	96.7%

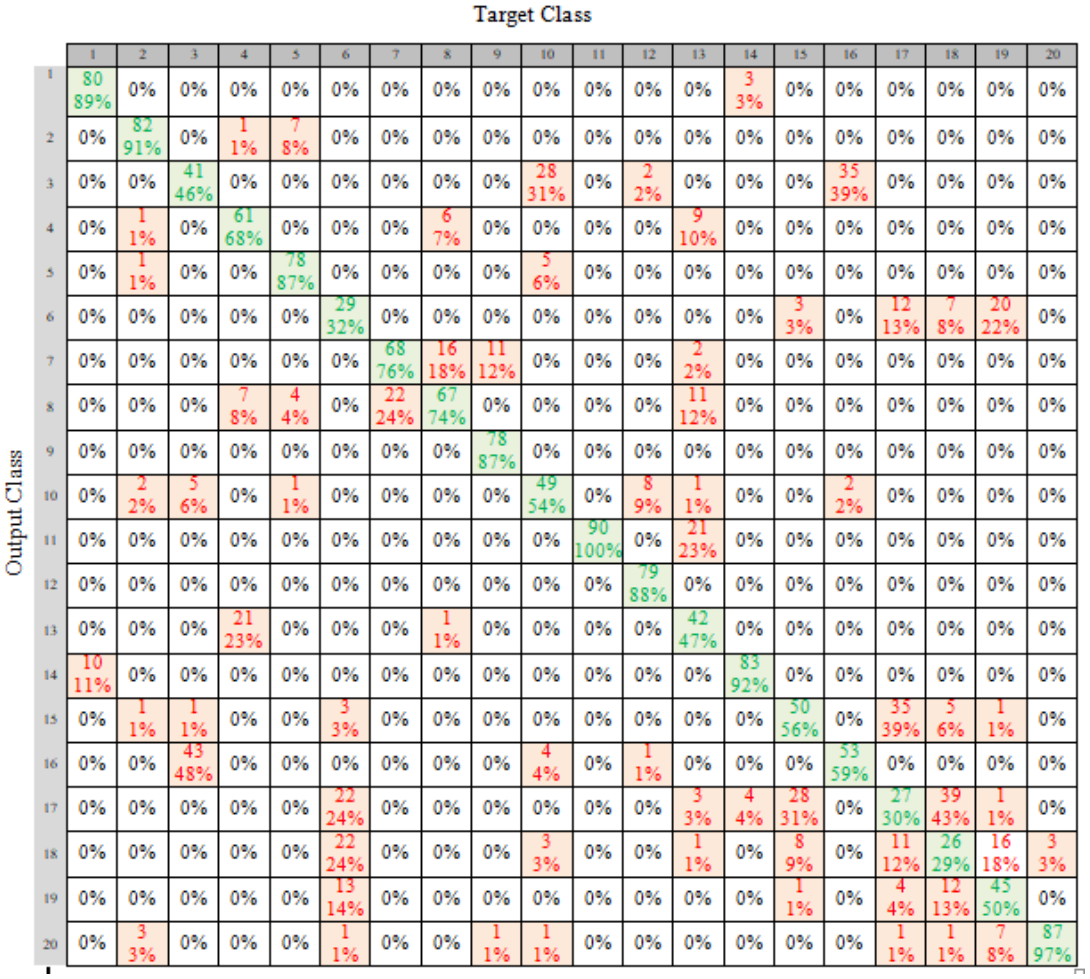

Figure 4.23 Confusion matrix of VMD- reconstructed transients

at SNR range (-5dB : 0dB)

Classification performance of VMD-modes method is better than VMD reconstructed method. Moreover, when device based performance is studied for VMD-reconstructed transient method, it was found that several of I-Phone models were misclassified (the lowest average classification rate of 59% was obtained) at moderate SNR level while the lowest correct classification average in VMD-modes method was located as 68% (the highest misclassified transients are of device 6 (IPhone 6S- B) which is mis-classified as class 5 (I-Phone 6S A)) see Fig. 4.25 and Fig. 4.26.

On the other hand from features representation in Fig. 4.21 we can note that features of deviec 5 and device 6 are completely overlapping while features created by VMD-modes Fig. 4.22 are nearly separated which is increased the performance classification about 4% with respect to VMD- reconstructed method.

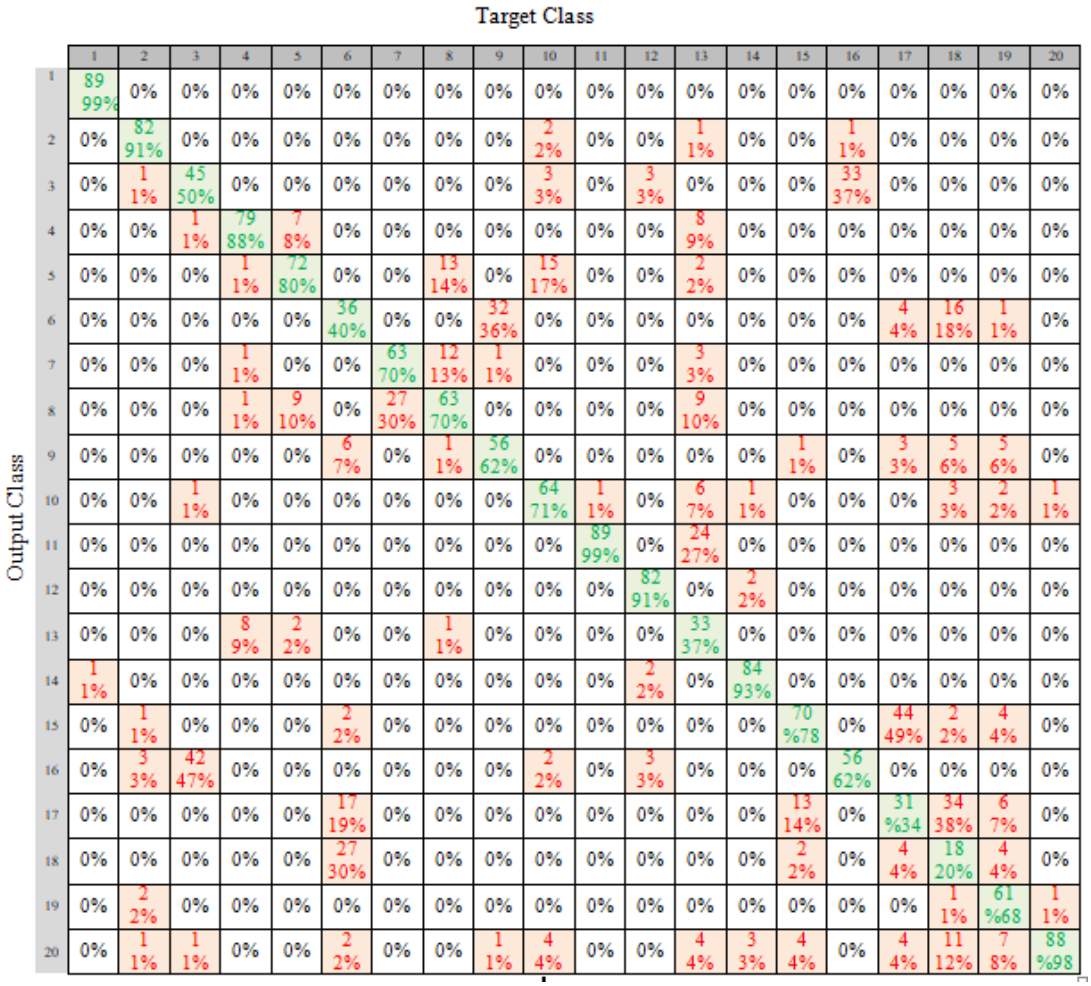

Figure 4.24 The confusion matrix of VMD-modes at SNR range (-5dB : 0dB)

Figure 4.25 The confusion matrix of VMD-reconstructed transients at SNR range (0dB : 5dB)

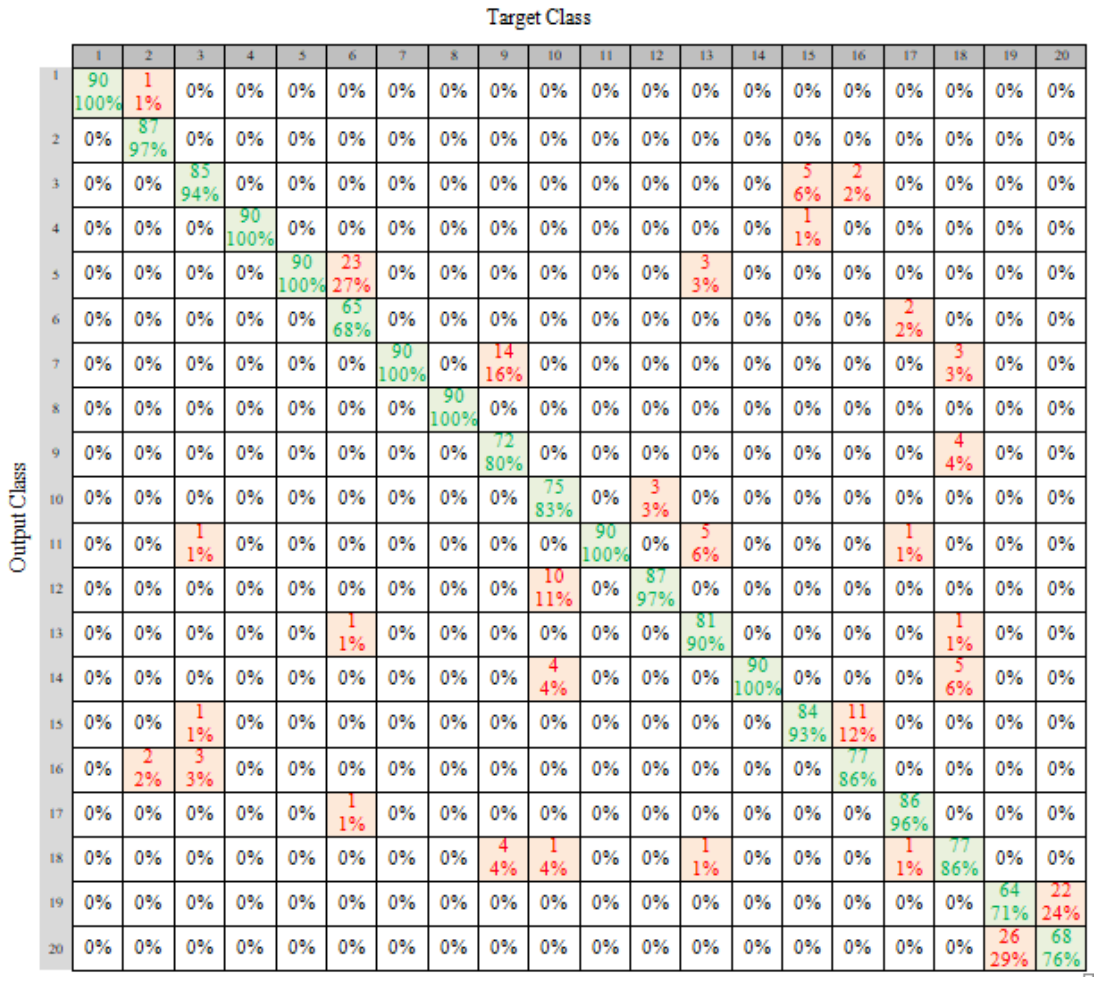

Figure 4.26 The confusion matrix of VMD- modes at SNR range (0dB : 5dB)

CHAPTER 5

CONCLUSION

In this study, noise robustness is considered to indicate the VMD efficiency in terms of noise presented in the input signal, we applied a series of simulation test signals under different important parameters such as lagrangian step time (τ), modes number (Z) and balancing parameter alpha (α). To demonstrate the performance of the VMD method for signal interrupt, we applied VMD to a simulation noisy signal consisting of three modes (Z=3). Since our goal is to eliminate noise from the input signal, it is not to get a exact reconstruction signal, the lagrangian multiplier is efficiently turned off by setting the value at zero, just selecting the time step $\tau = 0$. The appropriate value of the number of modes with (Z = 3) was selected. The achievement of the technique is measured in terms of (signal / noise) ratio (SNR) metric. Based on the simulation results, it is concluded that the strongest mode of low frequency is reconstructed clearly with high SNR (SNR=35dB) and the medium-strong signal is recovered with (SNR=17 dB), but the high frequency mode which is a weak signal is affected by the noise and the mode frequency is captured correctly (SNR=5 dB).

When the parameters (Z, α) have an inappropriate value, the results will affected. The effect of over- and under-segmentation of the given data is examined, by changing the values of the parameter (Z) into a few modes and many modes. For under-segmentation (Z=2), there will be sharing between the neighboring modes where some modes are contained in other modes for small alpha (α=100), or mostly discarded modes for big alpha ($\alpha = 10000$ and no Lagrangian multipliers).

On the other hand, when over-segmentation (Z=4), and small band width control parameter ($\alpha = 100$), one or several modes get noisy and broad spectral density. For large value of (α =10000), the center frequency of two or more modes get matched (mode duplication) and some of important parts of signal spectrum shared with others. This leads to the choice of parameters should be defined in advance to get strong robustness of VMD decomposition method.

Since too many of modes drive to unnecessary VMD information and few modes cause mode mixing in VMD results. Then, it is important to find the most appropriate mode (Z) value for the accuracy and efficient computation of the VMD. A combination of VMD and correlation coefficients (CCs) is used to minimize the number of modes (Z) and separate the simulation signal into intrinsic mode functions (IMF). Then the IMFs are separated into noisy IMFs and useful IMFs according to a selected threshold value of the CC. The noisy IMFs are discarded while the reconstructed useful IMFs are used in the denoising realization.

The performance of a VMD approach is measured over a simulation signal at different noise values ranging from -10 dB to 5 dB. The results demonstrate that the relationship between the input signal SNRs and the output signal SNRs is proportional to each other, if the input SNR increases the output SNR increases and the RMSE values decreases. The VMD method is implemented to the input noisy signal with different values of band width control parameter α, while keeping the other parameters fixed to measure the effect of α parameter on VMD performance. Output SNRs of denoised signal is increasing with increasing of (α) parameter and the relation between input SNRs and output SNRs is proportional, for high input SNRs, we have high output SNRs. Increasing the value of α will decrease the band width, which may causes a problem of not capturing the right center frequency, while the wide band width resulted by using too small α leads to noisy recovered modes.

In this work, we presented an identification method of Bluetooth devices based on the features of VMD-reconstructed transients. The method has three major stages: In the first stage, two models were selected for each mobile phone brand, and two mobile phones with various serial numbers were selected for each model. Therefore, a data set of twenty mobile phones containing one hundred and fifty transient signals was formed for each mobile phone. The formed transient signals are filtered by BPF and normalized before the detection process. The most popular transient detection method was based on the energy envelope of signal was used for transient detection in our study.

In the second stage, each Bluetooth transient signal is decomposed into a several band limited modes. Then these separated modes are added to generate the input transient signal. In the third stage, different statistical features are extracted such as variance, kurtosis and skewness. These features are created from the reconstructed transient signals and the decomposed modes of the transient signals. Nine features are created from each reconstructed transient signal and twenty seven features from decomposed modes (nine features of each mode). To illustrate the robustness of created features before applying the classifier, two types of plots are used, namely, box plot and conventional two dimensional Matlab plot. In the final stage, a LSVM classifier is used to classify the twenty BT classes (mobile phones) under various SNR condition. In order to test the performance at different SNR levels, the transient signals with SNR values of (5-10dB), (10-15dB) and (15-25dB) are created for testing. The classification performance demonstrated that the proposed technique obtained a high performance. We evaluated the performance of the proposed method on twenty mobile phones with 150 transients per device by using the correct classification percentage. There are many works related to our study but we chose Hilbert-Huang Transform (HHT) method as reference since this work shows the (HHT) performance with the same data set that we used in our work. In order to estimate the achievement of our proposed method, we make a comparison with the current (HHT) method in terms of correct classification average. Results show that our proposed VMD classification approach overcomes the existing (HHT) method at different ranges of SNR. The high performance of proposed method achieved because of advantages of VMD. Another advantage of this study is that we have used less features than the previous study (HHT), that uses more than 13 features but we have achieved better performance using only 9 features. On the other hand we studied an identification method for Bluetooth devices based on features of band-limited modes for BT transient signals. Band-limited modes are generated from BT transient signals by using variational mode decomposition (VMD).

Different statistical features are extracted from the band-limited modes, including variance, kurtosis and skewness. Twenty seven features (nine features of each mode) are extracted from the decomposed modes. The LSVM classifier is used to distinguish the twenty Bluetooth classes (mobile phones) under various SNR ranges (-5:0dB), (0:5dB) and (5:10dB) based on the features of modes. The obtained results demonstrate that the classification achievement of VMD-modes technique is better than VMD-reconstructed transients (4% higher accuracy). VMD-reconstructed transient is a sum of the band-limited modes which is generated by VMD. The identification improvement is due to the decomposed modes which include individual characteristics of the classes and also the number of features in the VMD-modes technique is bigger than that in VMD-reconstructed transient technique.

REFERENCES

[1] K. Youssef, L. Bouchard , K. Haigh, J. Silovsky, B. Thapa, and C. Vander, "Machine Learning Approach to RF Transmitter Identification," IEEE journal of radio frequency identification, vol. 2, no. 4, pp. 197-205, 2018.

[2] Q. Wu, C. Feres, D. Kuzmenko, D. Zhi, Z. Yu, and X. Liu, "Deep learning based RF fingerprinting for device identification and wireless security," Electronics letters, vol. 54, no. 24, pp. 1405-1407.

[3] M. Köse, S. Taşcioğlu, and Z. Telatar, "RF Fingerprinting of IoT Devices Based on Transient Energy Spectrum," IEEE Access, vol. 7, pp. 18715-18726, 2019.

[4] S. U. Rehman, K. W. Sowerby, and C. Coghill, "Radio - frequency fingerprinting for mitigating primary user emulation attack in low-end cognitive radios," IET Communications, vol. 8, no. 8, pp. 1274-1284, 2014.

[5] M. W. Lukacs, A. J. Zeqolari, P. J. Collins, and M. A. Temple, "RF-DNA Finger printing for Antenna Classification," IEEE antennas and wireless propagation letters,vol.14, pp. 1455-1458, 2015.

[6] K. Merchant, S. Revay, G. Stantchev, and B. Nousain, "Deep Learning for RF Device Fingerprinting in Cognitive Communication Networks," IEEE journal of selected topics in signal processing, vol. 12, no. 1, pp. 160-167, 2018.

[7] Y.-J. Yuan, Z.-T. Huang, and Z.-C. Sha, "Specific emitter identification based on transient energy trajectory," Progress In Electromagnetic Research C, vol. 44, pp. 67–82, 2013.

[8] C.-Y. Chen, K.-D. Chang, and H.-C. Chao, "Transaction pattern-based anomaly detection algorithm for IP multimedia subsystem," IEEE Transactions on Information Forensics and Security, vol. 6, no. 1, pp. 152–161, 2011.

[9] Y. M. Huang, M. Y. Hsieh, H. C. Chao, S. H. Hung, and J. H. Park, "Pervasive, secure access to a hierarchical sensor-based healthcare monitoring architecture in wireless heterogeneous networks," IEEE Journal on Selected Areas in Communications, vol. 27, no. 4, pp. 400–411, 2009.

[10] C.-S. Li, Y.-C. Tseng, H.-C. Chao, and Y.-M. Huang, "A neighbor caching mechanism for handoff in IEEE 802.11 wireless networks," Journal of Supercomputing, vol. 45, no. 1, pp. 1–14, 2008.

[11] L. Shu, M. Hauswirth, H.-C. Chao, M. Chen, and Y. Zhang, "Net Topo: A framework of simulation and visualization for wireless sensor networks," Ad Hoc Networks, vol. 9, no. 5, pp. 799–820, 2011.

[12] Z. Zhang, K. Long, and J. Wang, "Self-organization paradigms and optimization approaches for cognitive radio technologies: A survey," IEEE Wireless Communications., vol. 20, no. 2, pp. 36–42, Apr. 2013.

[13] K. Kim, C. M. Spooner, I. Akbar, and J. H. Reed, "Specific emitter identification for cognitive radio with application to IEEE 802.11," in Proc. IEEE GLOBECOM, pp. 1–5, 2008.

[14] B. W. Ramzey, T. D. Stubbs, B. E. Mullins, M. A. Temple, and M. A. Buckner, "Wireless infrastructure protection using low-cost radio frequency fingerprinting receivers," international journal of critical infrastructure protection, vol. 8, pp. 27-39, 2015.

[15] R. W. Klein, M. A. Temple, and M. J. Mendenhall, "Application of wavelet-based RF fingerprinting to enhance wireless network security," Journal of communications and networks, vol. 11, no. 6, pp. 544-555, 2009.

[16] T. J. Bihl, K. W. Bauer, and M. A. Temple, "Feature selection for RF fingerprinting with multiple discriminate analysis and using ZigBee device emissions," IEEE Transactions on information forensics and security, vol. 11, no. 8, pp. 1862-1874, 2016.

[17] Y. Tu, Z. Zhang, Y. Li, C. Wang, and Y. Xiao, "Research on the Internet of Things Device Recognition Based on RF-Fingerprinting," IEEE Access, vol. 7, pp. 37426-3743, 2019.

[18] J. H. Liang, Z. T. Huang, Z. W. Li, "Method of empirical mode decomposition in specific emitter identification," Wireless Pers Commun, vol. 96, pp. 2447–2461, 2017.

[19] O. Ureten and N. Serinken, "Wireless security through RF fingerprinting," Canadian Journal of Electrical and Computer Engineering, vol. 32, no. 1, pp. 27-33, 2007.

[20] W. C. Suski, M. A. Temple, M. J. Mendenhall, and R. F. Mills, "Using spectral fingerprints to improve wireless network security," IEEE Global Telecommunications Conference (GLOBECOM), pp. 1-5, 2008.

[21] K. Yang, J. Kang, J. Jang, and H. Lee, "Multimodal Sparse Representation-Based Classification Scheme for RF Fingerprinting," IEEE Communications Letters, pp. 1-4, 2019.

[22] J. M. McGinthy, L. J. Wong, and A. J. Michaels, "Groundwork for Neural Network-Based Specific Emitter Identification Authentication for IoT," IEEE Internet of Things Journal, pp. 1-13, 2019.

[23] J. Yu, A. Hu, G. Li, and L. Peng, "A Robust RF Fingerprinting Approach Using Multi-Sampling Convolutional Neural Network," IEEE Internet of Things Journal, pp. 1-14, 2019.

[24] C. Song, J. Xu, and Y. Zhan, "A method for specific emitter identification based on empirical mode decomposition," IEEE, pp. 54-57, 2010.

[25] W. Yang, Z. Peng, K. Wei1, P. Shi, and W. Tian, "Superiorities of variational mode decomposition over empirical mode decomposition particularly in time–frequency feature extraction and wind turbine condition monitoring," IET Renew. Power Generation., vol. 11, pp. 443-452, 2017.

[26] P. Shi and W. Yang, "Precise feature extraction from wind turbine condition monitoring signals by using optimized variational mode decomposition," IET Renew. Power Generation., vol. 11, pp. 245-252, 2017.

[27] K. Dragomiretskiy and D. Zosso, "Variational mode decomposition," IEEE Transaction Signal Process, vol.62, no.3, pp. 531-534, 2014.

[28] J. Long , X. Wang, D. Dai, M. Tian, G. Zhu, and J. Zhang, " Denoising of UHF PD signals based on optimized VMD and wavelet transform," IET Sci. Meas. Technol., vol. 11, pp. 753-760, 2017.

[29] U. Satija, N. Trivedi, G. Biswal, and B. Ramkumar, "Specific emitter identification based on variational mode decomposition and spectral features in single hop and relaying scenarios," IEEE Transactions On Information Forensics And Security, vol. 14, no. 3, pp. 581-591, 2019.

[30] C. Zhao et al, “Compressed Sensing Based Fingerprint Identification for Wireless Transmitters,” Scientific World Journal Volume 2014, Article ID 473178, 9 pages .

[31] S. Rehman et al, “RF Fingerprint Extraction from the Energy Envelope of an Instantaneous Transient Signal,” 2012 IEEE. Australian Communications Theory Workshop (AusCTW).

[32] G. Gok et al, “ Varyasyonel Kip Ayn§tlncl ile Radar Parmak izi (;lkarIffil Radar Fingerprint Extraction via Variational Mode Decomposition ,” (2017) IEEE.

[33] J.L. Padilla et al, “RF fingerprint measurements for the identification of device s in wireless communication networks based in feature reduction and subspace transformation,” Measurement 58 (2014) 468–475.

[34] B.W. Ramsey et al, “Wireless infrastructure protection using low - cost radio frequency fingerprinting receivers,” international journal of critical infrastructure protection 8(2015)27-39.

[35] C. Song et al, “Specific Emitter Identification Based on Empirical Mode Decomposition (EMD),” 2010 IEEE.

[36] C. Song et al, “Specific Emitter Identification Based on Intrinsic Time-scale Decomposition,” 2010 IEEE.

[37] J-H. Liang et al, “Empirical Mode Decomposition in Specific Emitter Identification,” Wireless Pers Commun (2017)96:2447-2461.

[38] X. An et al, “Analysis of hydropower unit vibration signals based on variational mode decomposition,” Journal of Vibration and Control 2017, Vol. 23(12) 1938–1953.

[39] A. Upadhyay and R. B. Pachori, “Instantaneous voiced-non voiced detection in speech signals based on variational mode decomposition,” Journal of Franklin Institute, vol. 352, pp. 2679-2707, 2015.

[40] B. He and Y. Bai, “Signal-Noise Separation of Sensor Signal Based on Variational Mode Decomposition,” 2016 8th IEEE International Conference on Communication Software and Networks.

[41] X. Bo Wang , et al, “Novel Particle Swarm Optimization-Based Variational Mode Decomposition Method for the Fault Diagnosis of Complex Rotating Machinery,” IEEE/ Transactions on Mechatronics, vol. 23, No. 1, February 2018.

[42] Y. Li, et al, “Research on Ship-Radiated Noise Denoising Using Secondary Variational Mode Decomposition and Correlation Coefficient,” www.mdpi.com/journal/sensors 2018, 18, 48.

[43] A. G. Asuero, et al, “The Correlation Coefficient" Department of Analytical Chemistry,” Faculty of Pharmacy, The University of Seville, Seville, 2016 Spain.

[44] A. M. Ali, E. Uzundurukan, and A. Kara, “Improvements on transient signal detection for RF fingerprinting,” presented at the Signal Processing and Communications Applications Conference, Antalya, Turkey, pp. 1–4, 2017.

[45] A. M. Ali, E. Uzundurukan, and A. Kara, “Assessment of features and classifiers for Bluetooth RF fingerprinting,” IEEE Access, vol. 7, pp. 50524-50535, 2019.

[46] Y. Yuan, Z. Hwang, H. Wu, and X. Wang, “Specific emitter identification based on Hilbert- Huang transform - based time-frequency-energy distribution features,” IET Communications., vol. 8, pp. 2404–2412, 2014.

[47] R.W. Klein, M.A. Temple, M.J. Mendenhall, “Application of wavelet-based RF fingerprinting to enhance wireless network security,” Journal of Communications and Networks, vol. 11, (2009), p.544-555.

[48] M.D. Williams, S.A. Munns, M.A. Temple, M.J. Mendenhall, “RF-DNA fingerprinting for airport WiMax communications security,” 4th International Conference on Network and System Security (NSS), (2010), p.32-39.

[49] D.R. Reising, M.A. Temple, M.J. Mendenhall, “Improving intra-cellular security using air monitoring with RF fingerprints,” Wireless Communications and Networking Conference ,(2010), p.1-6.

[50] P. Harmer, M.A. Temple, M. Buckner, E. Farquhar, “4G security using physical layer RF-DNA with de-optimized LFS classification,” Journal of Communications, vol. 6, (2011), p.671-681.

[51] J. L. Hintze, “Chapter 152 Box plots number cruncher statistical systems,” Hintze, Jerry L. "User’s Guide V." (2007).

[52] J. C Burges, “A tutorial on support vector machines for pattern recognition,” Data Mining and Knowledge Discovery, 121– 167, 1998.

[53] E. Bermani, A. Boni, A. Kerhet, and A. Massa, “Kernels evaluation of SVM-based estimators for inverse scattering problems,” Progress In Electromagnetic Research, Vol. 53, 167– 188, 2005.

[54] E. Bermani, A. Boni, S. Caorsi, M. Donelli, and A. Massa, “A multi-source strategy based on a learning-by-examples technique for buried object detection,” Progress In Electromagnetic Research, Vol. 48, 185–200, 2004 .

APPENDIX A

VMD CODE

```
function [f1_hat,u, u_hat, omega,xr] = VMD(t1,T1,f1, alpha,Z)


N = 500;tol = 1e-7;    tau = 0;   DC = 0;
f1_hat = fftshift((fft(f1)));
f1_hat_plus = f1_hat; f1_hat_plus(1:T1/2) = 0;
 % extend the signal by mirroring
f_mirror(1:T1/2) = f1(T1/2:-1:1);
f_mirror(T1/2+1:3* T1/2) = f1;
f_mirror(3* T1/2+1:2* T1) = f1(T1:-1: T1/2+1);
f = f_mirror;
% Time Domain 0 to T (of mirrored signal)
T = length(f);
t = (1:T)/T;
freqs = t-0.5-1/T;
Alpha = alpha*ones(1,Z);
f_hat = fftshift((fft(f)));    f_hat_plus = f_hat;     f_hat_plus(1:T/2) = 0;
u_hat_plus = zeros(N, length(freqs), Z);
omega_plus = zeros(N, Z); % Initialization of omega_z
lambda_hat = zeros(N, length(freqs));
uDiff = tol+eps; n = 1; sum_uz = 0;
 while ( uDiff > tol &&  n < N )
z = 1;
sum_uz = u_hat_plus(n,:,Z) + sum_uz - u_hat_plus(n,:,1);
 u_hat_plus(n+1,:,z) = (f_hat_plus - sum_uz -
lambda_hat(n,:)/2)./(1+Alpha(1,z)*(freqs - omega_plus(n,z)).^2);
    % update first omega if not held at 0
 omega_plus(n+1,z) =0;
```

```
for z=2:Z
 sum_uz = u_hat_plus(n+1,:,z-1) + sum_uz - u_hat_plus(n,:,z);
u_hat_plus(n+1,:,z) = (f_hat_plus - sum_uz -
lambda_hat(n,:)/2)./(1+Alpha(1,z)*(freqs - omega_plus(n,z)).^2);
% center frequencies
omega_plus(n+1,z) = (freqs(T/2+1:T)*(abs(u_hat_plus(n+1, T/2+1:T,
z)).^2)')/sum(abs(u_hat_plus(n+1,T/2+1:T,z)).^2);
 end

 % Dual ascent
 lambda_hat(n+1,:) = lambda_hat(n,:) + tau*(sum(u_hat_plus(n+1,:,:),3) -
f_hat_plus);
 n = n+1;   uDiff = eps;
 for i=1:Z
 uDiff = uDiff + 1/T*(u_hat_plus(n,:,i)-u_hat_plus(n-1,:,i))*conj((u_hat_plus(n,:,i)-
u_hat_plus(n-1,:,i)))';
 end
 uDiff = abs(uDiff);
 end

%------ Post processing and cleanup
N = min(N,n); % discard empty space if converged early
omega = omega_plus(1:N,:);
% Signal reconstruction
u_hat = zeros(T, Z);
u_hat((T/2+1):T,:) = squeeze(u_hat_plus(N,(T/2+1):T,:));
u_hat((T/2+1):-1:2,:) = squeeze(conj(u_hat_plus(N,(T/2+1):T,:)));
u_hat(1,:) = conj(u_hat(end,:));
u = zeros(Z,length(t));     %   size 2000
for z = 1:Z
 u(z,:)=real(ifft(ifftshift(u_hat(:,z))));
 end
u = u(:,T/4+1:3*T/4); % remove mirror part
```

```
% recompute spectrum
clear u_hat;xr=0;
for z = 1:Z
 u_hat(:,z)=fftshift(fft(u(z,:)))';
 xr=xr+(u(z,:));
 end

%---------- Visualization
% For convenience here: Order omegas increasingly and reindex u/u_hat
[~, sortIndex] = sort(omega(end,:));
omega = omega(:,sortIndex);
u_hat = u_hat(:,sortIndex);
u = u(sortIndex,:);
 figure('Name', 'Composite input signal' );
 plot(t1,f1, 'z');
 set(gca, 'XLim', [0 1]);
 figure('Name', 'Input Transient spectrum' );
 loglog(freqs1(T1/2+1:end), abs(f1_hat(T1/2+1:end)), 'z');
 set(gca, 'XLim', [1 T1/2]*pi*2, 'XGrid', 'on', 'YGrid', 'on', 'XMinorGrid', 'off',
'YMinorGrid', 'off');
 ylims = get(gca, 'YLim');
 hold on;
 set(gca, 'YLim', ylims);
 figure('Name', 'Evolution of center frequencies omega');
 for z=1:Z
 semilogx(2*pi/(1/T1)*omega(:,z), 1:size(omega,1), linestyles{z});
 hold on;
 end
 set(gca, 'YLim', [1,size(omega,1)]);
 set(gca, 'XLim', [2*pi,0.5*2*pi/(1/T1)], 'XGrid', 'on', 'XMinorGrid', 'on');

 figure('Name', 'Spectral decomposition');
 loglog(freqs1(T1/2+1:end), abs(f1_hat(T1/2+1:end)), 'z:');
```

```
 set(gca, 'XLim', [1 T1/2]*pi*2, 'XGrid', 'on', 'YGrid', 'on', 'XMinorGrid', 'off',
'YMinorGrid', 'off');
 hold on;

for z = 1:Z
 loglog(freqs1(T1/2+1:end), abs(u_hat(T1/2+1:end,z)), linestyles{z});
 end
 set(gca, 'YLim', ylims);

  for z = 1:Z
 figure('Name', ['Reconstructed mode ' num2str(Z)]);
 plot(t1,u(z,:), linestyles{z});   hold on;
  end

 figure('Name', 'Reconstructed Transient' );
 plot(t1,xr, 'z');
 set(gca, 'XLim', [0 1]);
```